NSF/CEE-82135

PB84-178961

Final Report

on the

Tomographic Assessment Techniques for Earthquake Engineering

National Science Foundation
Award Number CEE 8113999
Phase I

Submitted by

Scientific Measurement Systems, Inc.

2808 Longhorn Boulevard

Suite 303

Austin, Texas 78759

March 31, 1982

This material is based upon work supported by the National Science Foundation under award number CEE 8113999. Any opinions, findings, and conclusions or recommendations expressed in this publication are those of the authors and do not necessarily reflect the views of the National Science Foundation.

50272-101

REPORT DOCUMENTATION PAGE	1. REPORT NO. NSF/CEE-82135	2.	3. Recipient's Accession No. PB84 178961

4. Title and Subtitle
Tomographic Assessment Techniques for Earthquake Engineering, Final Report

5. Report Date
March 1982

6.

7. Author(s)
None listed

8. Performing Organization Rept. No.

9. Performing Organization Name and Address
Scientific Measurement Systems, Inc.
2808 Longhorn Boulevard, Suite 303
Austin, TX 78759

10. Project/Task/Work Unit No.

11. Contract(C) or Grant(G) No.
(C)
(G) CEE8113999

12. Sponsoring Organization Name and Address
Division of Industrial Science and Technological Innovation(ISTI)
Directorate for Scientific, Technological, and International Affairs (STIA)
National Science Foundation, Washington, DC 20550

13. Type of Report & Period Covered
SBIR-Phase I

14.

15. Supplementary Notes

16. Abstract (Limit: 200 words)

Results are presented of an investigation of the feasibility of applications of the Computerized Tomographic (CT) and the Compton Interaction Tomographic (CIT) processes to the nondestructive testing and evaluation of reinforced concrete components integral to many massive structures. The CT techniques were examined on a specially designed object incorporating various mass densities, cracks of varying dimensions, rebars, and air voids. It is concluded that these techniques are applicable to the nondestructive examination of massive structures. The CIT techniques were examined on a specially designed apparatus, with an aim to detect rebars and air voids embedded within a medium. The results of this study indicate the possibility of applications of this technique for the examinations of extended systems, such as highways and walls.

17. Document Analysis a. Descriptors

Earthquakes
Assessment
Structures
Tests
Evaluation
Reinforced concrete
Nondestructive tests
Dynamic structural analysis
Structural members

b. Identifiers/Open-Ended Terms
Tomography

I.L. Morgan, /PI

c. COSATI Field/Group

18. Availability Statement:	19. Security Class (This Report)	21. No. of Pages
NTIS	20. Security Class (This Page)	22. Price

(See ANSI-Z39.18) See Instructions on Reverse

OPTIONAL FORM 272 (4-77)
(Formerly NTIS-35)
Department of Commerce

Table of Contents

1. Introduction

Nondestructive testing and evaluation (NDT, NDE) techniques are in great demand in many diverse fields of activity. A particularly important area of interest warranting an efficient, rapid and accurate NDT/NDE technique is encountered in the reinforced concrete structural components integral to many massive structures. Among other things, damaged or defective components in a structure pose a potential for hazard as well as inadvertent economic losses in the event of an earthquake. An efficient NDT/NDE technique for evaluating the status of such components, not only at the time of construction but also periodically, is therefore indispensable. There are numerous other areas of interest where there is a great need for NDT/NDE for quality control, and maintainance surveillance to aid not only in assuring the operational worthiness of a system but also in reducing the potential for hazard as well as reducing inadvertent economic losses.

Computerized tomography is one of the NDT/NDE techniques which essentially provides an innovative three dimensional imaging process. It has already received a broad application and an extensive research and development in the field of medical diagnostics. Although it has found significant applications in the industrial areas of interest encompassing a wide range of massive objects, it has received less attention in the area of research and development. In this study we have undertaken to investigate the feasibility of the application of CT processes for NDT and NDE of structures to rapidly and accurately detect and assess the defects and/or damages such as cracks, voids, delaminations, corrosions, etc., commonly encountered in reinforced concrete components of a structure.

The physical principles underlying CT processes are the principles governing the interactions between electromagnetic radiation and matter. In this investigation two forms of tomographic processes are considered. One is termed Photon Transmission Tomography and is the usual kind of computerized tomography, and the second one termed as Compton Interaction Tomography, (CIT), is a new, innovative approach to the three dimensional imaging of an extended system. CT techniques are most suited for object systems of permitting a 360^{o} access. When the system is of such dimensions as to prohibit a 360^{o} access, use of CT process would permit only a limited sampling and the consequent lack of detailed information. For such systems CIT would provide a good approach for inspecting extended objects.

To assess the feasibility of these techniques we have chosen to examine a specially fabricated object - a phantom - through these techniques. The phantom was designed to incorporate a range of densities varying from $\sim$0 gm/cc (air) to $\sim$ 7.87 gm/cc (stainless steel). It contained features of interest such as cracks of varying thicknesses, air voids of varying sizes, steel rebars, concrete composition, aggregate and sand. CT examination was conducted with the use of a 50 Ci ^{60}Co as the photon source whereas the CIT technique was tested with a 25 Ci ^{192}Ir source. In testing the CT technique several tomographic parameters of importance, namely the number of angular views, the ray spacings in the fan beam and the degree of collimation, were varied to examine the influence of these parameters on the quality of results i.e. the spatial resolution obtained.

This report is organized as follows. In Section 2, a brief discussion of theoretical background of these techniques is presented. Details of the tomographic setups are included in Section 3. Section 4 contains the description of the tomographic examinations and a discussion of the results obtained. All pertinent details of the outcome of this project are summarized in Section 5.

2. Theoretical Background

Tomography is essentially based on the phenomena of interaction between electromagnetic radiation and matter. When a beam of gamma rays is transmitted through an object, it is well known that the transmitted intensity, (T), is related to the incident intensity, (I), through the relation

$$T = I\, e^{-\mu . x} \tag{1}$$

where μ is the linear attenuation coefficient, characteristic of the medium and x is the thickness of the material. Eq. 1 implicitly assumes that the radiation is monochromatic and the medium is homogeneous.

There are several physical processes through which the photon beam may be attenuated. However, there are three principal interactions which are significant over different ranges of photon energies: (1) Photoelectric capture (0.01 MeV - 0.5 MeV), (2) Compton Scattering (0.05 MeV), and (3) Pair production (1.02 MeV and above). For the energies under consideration ($\ll$1.3 MeV), photoelectric and Compton processes are dominant, and the contribution of pair production process to the beam attenuation is less than 1%. The linear attenuation coefficient, μ, in Eq. 1, is the combination of attenuation obtained through these three processes. Physical principles underlying these processes are well discussed in literature [2,3] and hence we shall omit a discussion of these. We may summarize the three processes by the relation,

$$\mu_{TOT} = \left\{ \frac{\rho N_A}{A} \right\} \left\{ \mu_{PE} + \mu_C + \mu_{PP} \right\} \tag{2}$$

where μ_{PE}, μ_C and μ_{pp} are the atomic attenuation coefficients due to photoelectric, Compton and pair production processes respectively and are given

approximately by relations:

$$\mu_{PE} \sim K_{PE} \cdot Z^{4.5} / E^3$$
$$\mu_C \sim K_C \cdot f(E) \cdot Z$$
$$\mu_{PP} \sim K_{PP} \cdot Z^2 \cdot g(E) \qquad (3)$$

where K's are constants and, f(E) and g(E) are photon energy dependent factors. ρ is the density; N_A, Avagadro's number, Z the atomic number, and A the atomic weight.

We may note in passing that Compton process is ideally suited for producing electron density information since it is proportional to Z.

The transmission relation, Eq. 1, in view of Eq. 3, is a function of photon energies. Generalizing this for a non-homogeneous medium, we have the transmitted intensity dependent also upon the position for radiation incident in a specific direction.

$$T(x,E) = I(x_o,E)\, e^{-\int_{x_o}^{x} \mu(t,E)\cdot dt} \qquad (4)$$

where t is the co-ordinate measured in the direction of the incident radiation and μ is the linear attenuation coefficient. The total absorption at a given energy of incident photons, along a line from x_o to x is given by

$$\int_{x_o}^{x} \mu(t,E)\,dt = \ln \frac{I(x_o,E)}{T(x,E)} \qquad (5)$$

Notice that μ, the linear attenuation coefficient is a function of the material properties of the object under examination and hence if the photon energy,

E, is known, it contains the information on the material properties of the object. Ignoring the photoelectric effect, the function $\mu(x,E)$ may be approximated using Eq. 2 as,

$$\mu(x,E) \simeq \left[\frac{\rho(x)\, Z(x)\, N_A}{A(x)}\right]\left[K_{PE}\, Z^{3.5}(x)/E^3 + K_c f(E)\right] \tag{6}$$

The first factor in parentheses represents the electron density at position x along the ray. Rewriting Eq. 5, we have,

$$\int_{x_o}^{x} e_d(t)\left\{K_{PE}\cdot Z^{3.5}(t)/E^3 + K_c f(E)\right\} dt = \ln \frac{I(x_o,E)}{T(x,E)} \tag{7}$$

where $e_d(x)$ is the electron density.

Eq. 7 may be generalized to two dimensions to mathematically analyze the tomographic "reconstruction" process. For describing attenuation along a scan line in any section ("tomos") of an object, consider the following equation: (See Fig. 1)

$$L(b,\varphi,E) = \int dr \int d\theta\; e_d(r,\theta)\cdot r\cdot \delta(b - r\cos(\theta-\varphi))\cdot \cdot\left\{K_{PE} Z^{3.5}(r,\theta)/E^3 + K_c f(E)\right\}$$

where

$$L(b,\varphi,E) = \ln\left\{ I_o(b,\varphi,E)/T(b,\varphi,E)\right. \tag{8}$$

φ is the inclination of the scan line with the x-axis (polar axis) and b is the perpendicular distance from the origin to the line. Inversion of Eq. (8) is the essential basis for reconstruction of the object plane in which the transmission data are collected. In absence of photoelectric effect, inversion of Eq. 8 produces electron density map for a given object plane and is closely related to the mass density distribution of the object.

Eq. 8 represents a relationship for an ideal case consisting of point sources and point detectors. In practice, both the source as well as the detectors have finite apertures and hence the information obtained for transmission is over a strip of finite area rather than for a ray. Consequently the degree of detail obtainable through the reconstruction of the object function is limited. In addition to this there are numerous sources of errors and uncertainties which exist in any particular tomographic set up. For the sake of brevity we omit a discussion of these and state that over past years, SMS, Inc. has developed various computer algorithms to reconstruct object functions from transmission data and implement a number of error correction and data smoothing techniques.

In most systems requiring nondestructive testing and evaluation, an important criterion for assessing the applicability of a technique includes the accuracy obtainable on the required information as a function of time required for measurement and processing. In tomography the parameters constraining the amount of information obtained are (i) the number of scan views and (ii) the number of rays in a given beam (i.e. the number of detectors). The quality of the information depends on parameters such as the isotopic gamma ray source strengths, collimation of the source and the detector, and the exposure times. Thus investigation on the accuracy of results in tomographic examination is synonymous with the concept of assessing "resolving power" of the system.

Reconstruction of an object function in the fashion described above is applicable to objects permiting a 360^{o} excess for scanning. For objects of physical extents prohibiting a 360^{o} excess, the usual tomographic process would yield only partial information. For such cases there is an attractive and innovative approach for collecting data on the interior of an object based on the principle of Compton interactions.

As discussed earlier the linear attenuation coefficient arising out of the Compton interaction process is directly proportional to Z, the atomic number. Hence it is in direct proportion to the electron density of the medium at the point of interaction.

The essential content of Compton backscatter theory is that a photon of frequency ν, scattering off an electron at an angle φ will experience a characteristic shift in the frequency given by the relation

$$\nu' = \frac{\nu_0}{1 + \alpha(1 - \cos\varphi)} \tag{9}$$

where ν' is the frequency of the scattered photon and $\alpha = h\nu_0/m_0c^2$ is the incident photon energy normalized with respect to the electron rest mass energy. For a given incident intensity of the photon beam the intensity of the backscattered beam at a given angle depends upon the probability for an interaction to take place. This is termed the Compton scattering cross-section and is a function of the incident frequency as well as the scattering angle.

The total probability then depends on the volume density of electrons contained in the medium. In addition to these factors the backscattered beam undergoes attenuation of the usual kind explained earlier in this section. The frequency shift, Compton cross-section and the total attenuation in the medium are dependent on the geometry of the beam paths as well as the incident photon energy. Fig. 2 shows a diagram of the Compton interaction process whereas in Fig. 3 we include a typical Compton interaction tomographic setup.

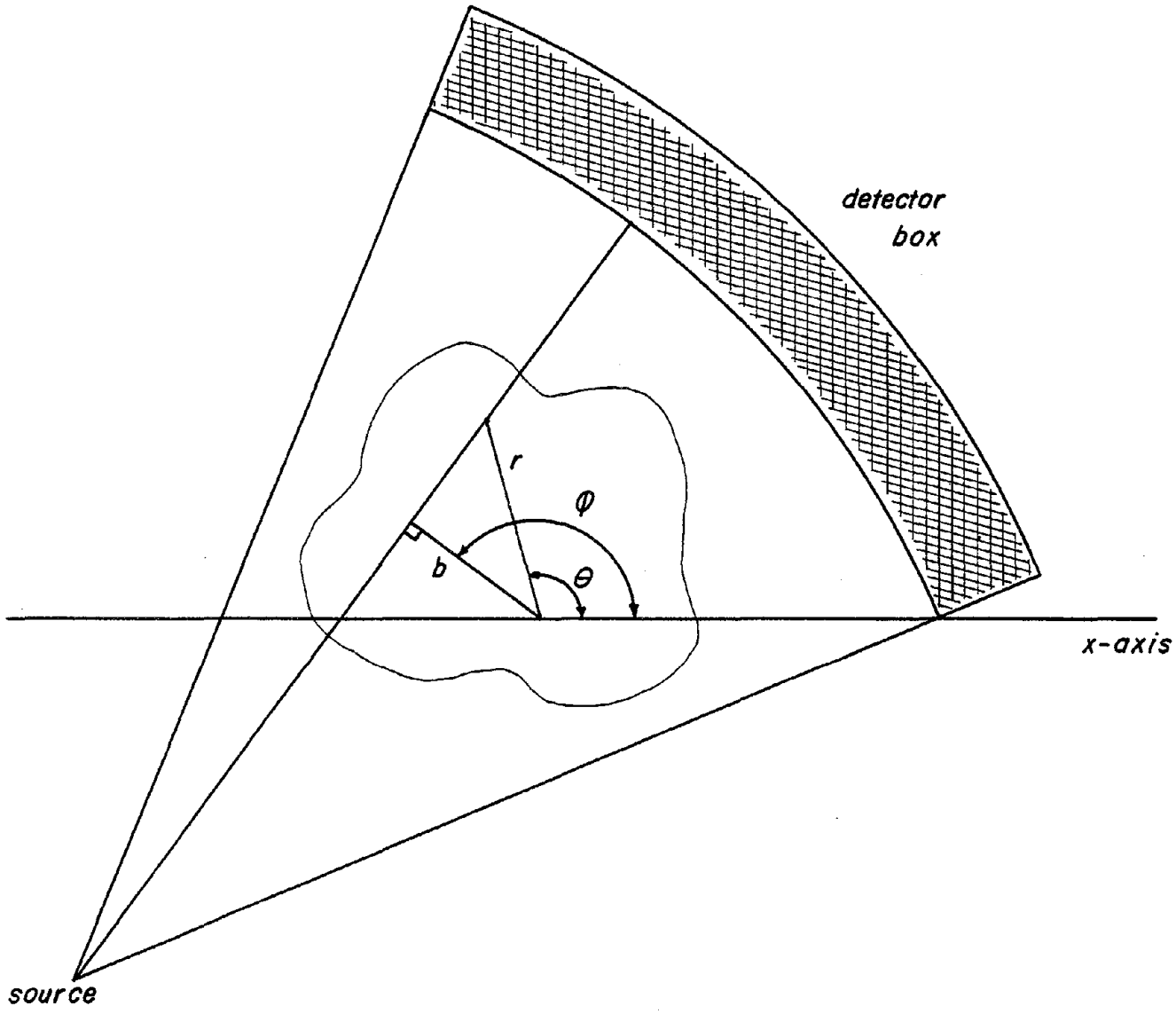

Figure 1

COMPTON INTERACTION TOMOGRAPHY

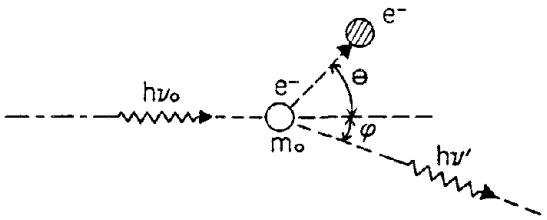

Scattered photon energy

$$h\nu' = \frac{h\nu_0}{1+\alpha_0(1-\cos\varphi)}$$

α_0= normalized incident energy = $\frac{h\nu_0}{m_0c^2}$

proabability of scattering at an $\measuredangle \varphi$
proportional to the electron density
of the medium.

Figure 2

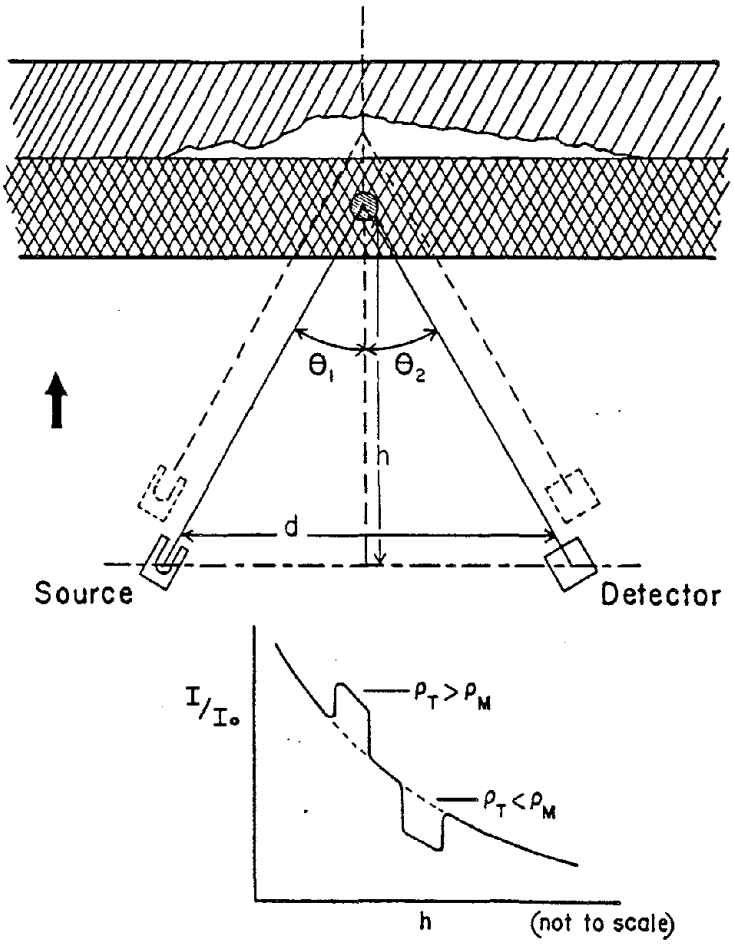

Fig. 3. A typical CIT set-up. The graph shows the variation in the back-scattered intensity normalized to the incident one as a function of the depth in the material. A rise in (I/I_o) is obtained when the electron density of the target is greater than the material background and the converse for the lesser electron density target.

3. Tomographic Setup

The SMS EM-1 laboratory tomographic scanner has been in successful operation for over four years. It is configured in a fan beam geometry with a source to detector distance of 122 cm, as shown in Fig. 4. The detector system consists of 31 individual NE102 scintillation detectors coupled to phototubes, all housed in a light-tight aluminum box. Phototube output is processed in the pulse (photon) counting mode with amplifier/discriminators and recorded digitally in scalers. Cross-sectional dimensions of the detectors are 6.4 mm width and 20.0 mm height with lengths from 125 mm to 250 mm, aligned radially from the source. The beam flux can be collimated to a width of 2.4 mm and a height of 2.00 mm at each detector by lead detector apertures with the interdetector spacings of $\sim$ 8 mm boundry to boundry.

The photon source used in scanning is a 50 Ci Cobalt-60 source housed in a standard radiographic device. Without the collimator the beam flux produces a count-rate of $\sim$ 10 MH_Z in the detectors with no object intercepting the flux. The background count-rate with appropriate phototube voltages and thresholds averages a few hundred hertz. Source collimation restricts the primary flux to a solid angle which falls within that defined by a highly absorptive front face of the lead collimator assembly. In this configuration the scattering is minimized. The height of the fan beam at the center of the source-detector separation is $\sim$ 5 mm.

The object table is normally positioned halfway between the source and the detector, with a provision for locating it either closer to the source or to the detector. The current SMS EM-1 scanner operated as a modified "third-generation" rotate-only tomograph. Given a fixed orientation of source and detector bank, the object table can be rotated through 360^{o}, with data

accumulation occurring at specified regularly spaced angles within that range. These positions are termed as "views". The detector bank is then stepped sequentially to other positions within the angle defined by the axes of consecutive detectors, and the object rotation procedure is repeated at each of these detector bank positions. In this manner the density of ray paths defined within the fan beam is increased to any desired number up to 512.

As is evident from Fig. 4, the entire data taking process with the exception of vertical positioning of the object, (i.e. selection of a particular cross-section of the object) is accomplished automatically under control by a data acquisition program residing in the SMS-PDP 11/35. Positioning of the detector box, rotation of the object table, and periodic interrogation of the scalers recording the detection signals are performed in the above manner. Calibrations, including alignment of the detector bank to insure proper geometry and recording detector counts with no object in place (i.e. "air count") for normalizing transmission counts, are completed prior to data accumulation.

For the present study data were taken for 6 equally spaced positions of the detector box over the interval of 1.38 cm. Consequently adjacent rays in the fan beam subtended an angle of 0.108°, producing a ray spacing at the center of rotation of the object of 1.15 mm. At each detector position data were obtained about 360° at regular angular increments of 0.5625° providing a total of 640 angular positions. Effectively these produced 295,680 individual ray measurements requiring approximately 8.5 hours for data collection.

The setup for the Compton interaction tomographic studies was specially designed. The schematics of this setup are shown in Fig. 5. The system basically consists of a radioactive photon source, a detector system and an object table capable of translatory movement.

The source consists of a 25 Ci ^{192}Ir housed in a standard radioactive shielding device. A collimator made of an 8" x 4" x 4" lead block with 1 cm x 1 cm aperture is added in front of the source. The detector system consists of a cylindrical NaI crystal, 1.5" in diameter and 1.5" long, connected to a photomultiplier tube base. It is shielded with $\sim$1" thick lead plates and the collimation device used is identical to the one used for the source. The signal from the detector is amplified via a Canberra 1417 spectroscopy amplifier and is processed through a LeCroy QVt multichannel pulse-height analyzer. The multichannel analyzer is interfaced to the PDP 11/35 computer through a LeCroy QVt Camac interface.

The object table consists of a 14" x 14" movable carriage. The carriage can be moved forward or backward by a stepping motor mechanism which is computer controlled. It can support as much as 500 lbs., and has a maximum permissible displacement of 16 inches with a positioning accuracy of 0.01 mm.

The object table positioning, data collection and analysis are accomplished through the software developed by SMS for backscattering studies. All of the experimental steps are automated except for the source and the detector positioning and orientation.

TOMOGRAPHIC SCANNING SYSTEM

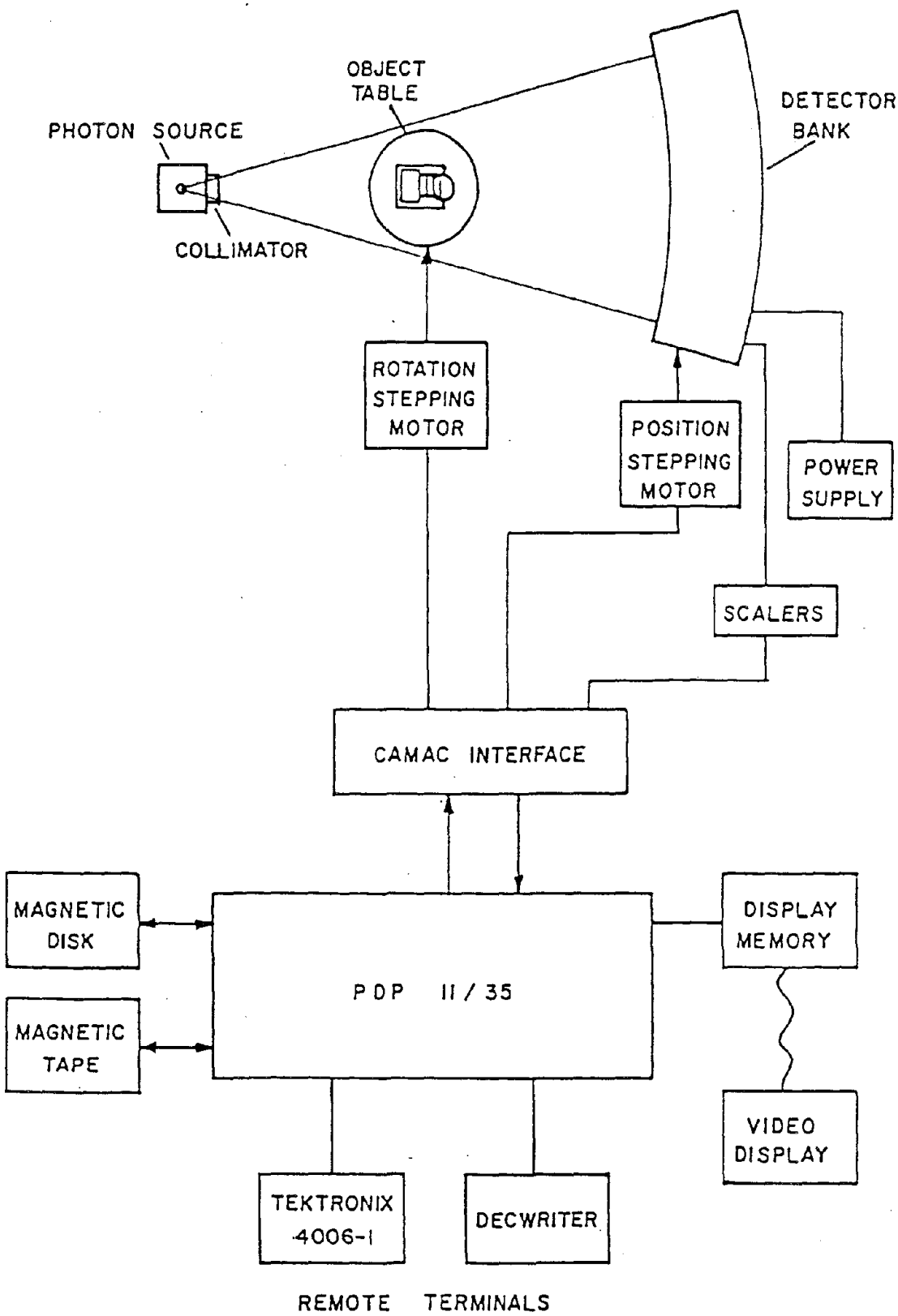

Figure 4

Figure 5. COMPTON INTERACTION TOMOGRAPHIC SCANNING SYSTEM

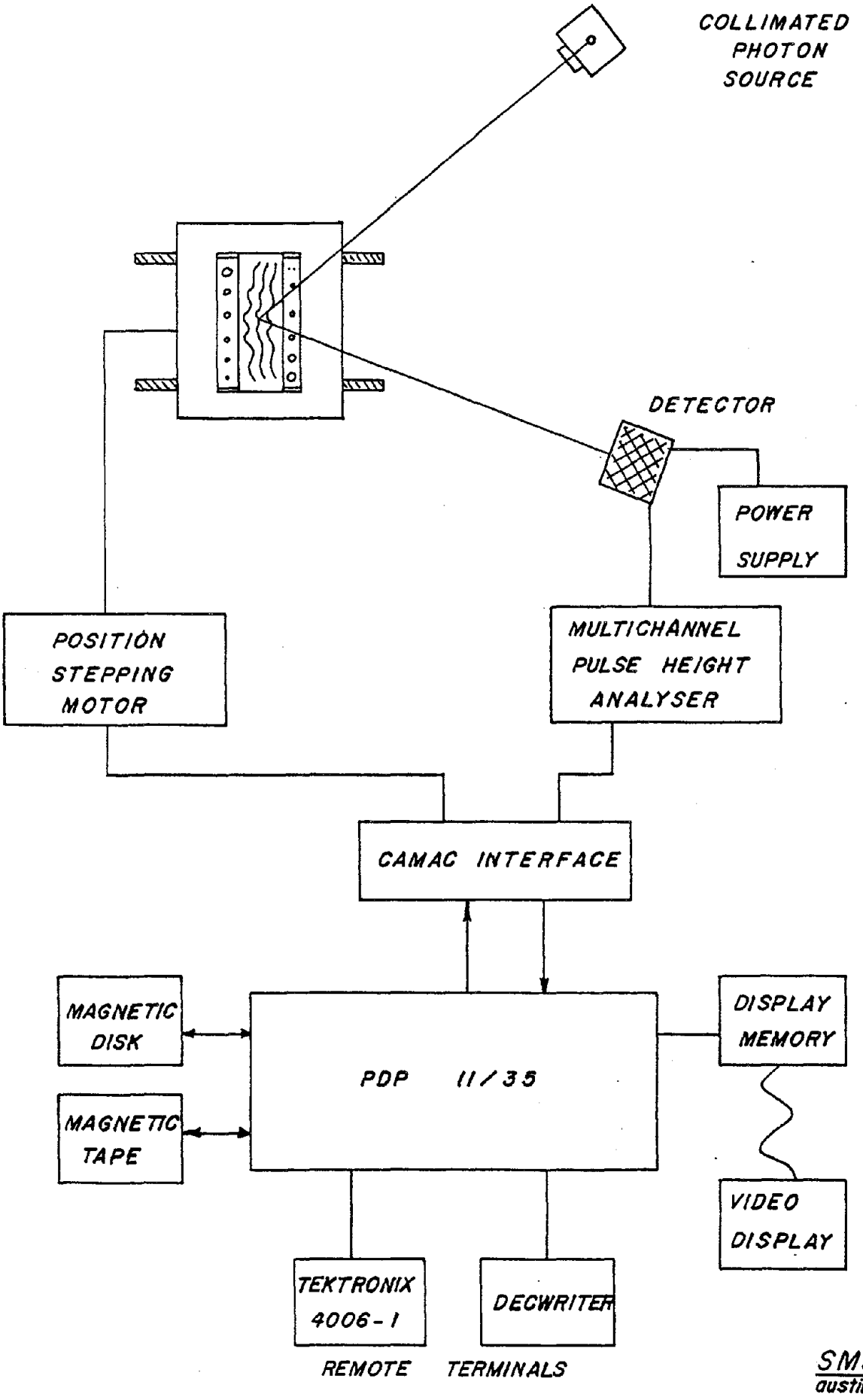

4. Tomographic Examination

(a) Description of the phantom.

To investigate the feasibility of CT and CIT processes as efficient and accurate techniques for nondestructive testing of systems susceptible to earthquake damages, we have constructed a special object for examination.

The object fabricated was designed to contain special features such as a range of mass densities and defects such as cracks and voids. A diagram of this object is presented in Figure 6. It consists of a row of rebars of varying diameters (from 1" to 3/16"),a series of air voids simulated by aluminum pipes of varying inner diameters (1/8" to 1") and a concrete block possessing cracks of thicknesses 1/8" to 1/2". The shape of these cracks was specifically designed to simulate nonlinear characteristics of cracks typically encountered in a medium. These components were contained in a 14" x 18" x 6" wooden box with the intervening region filled with a mixture of sand and aggregate taken in equal proportions by weight. Materials were chosen to closely simulate those typically encountered in construction.

(b) Tomographic examination and analysis.

Tomographic examination of an object essentially involves reconstruction of a cross-sectional map of the object interior through the plane of examination. Such a reconstruction is termed a "tomogram". The quality of a tomogram is judged by the spatial resolution obtained for the features of interest. In this section we discuss the details of various tomograms obtained. Specific cases considered are (i) the influence of collimation, (ii) the influence of the limited view scanning and (iii) the influence of the number of angular views and the ray spacings. These three cases are discussed and analyzed separately below.

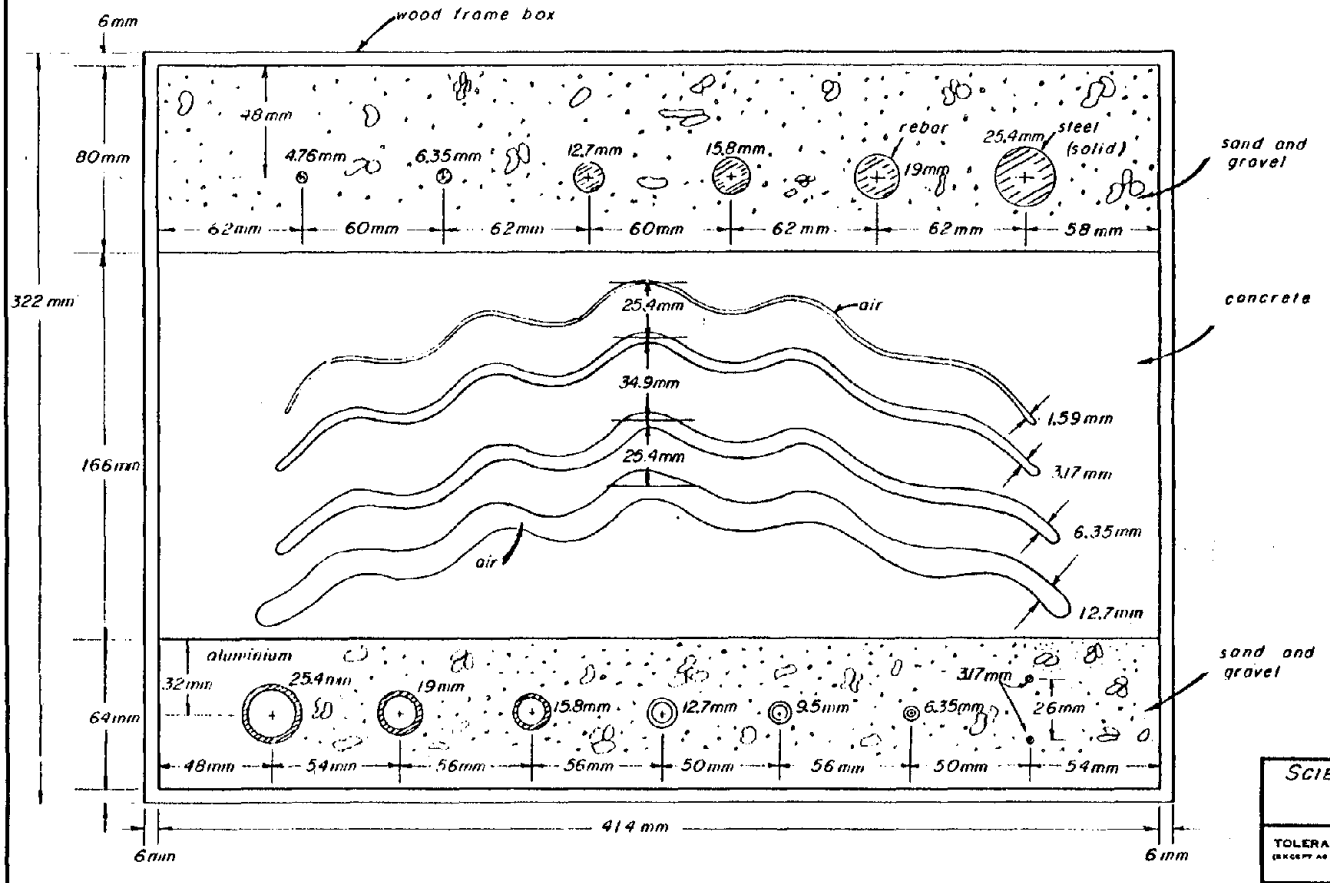

DATE	SYM	REVISION RECORD	AUTH.	DR.	CK.

SCIENTIFIC MEASUREMENT SYSTEMS INC.
austin, texas

TOLERANCES (EXCEPT AS NOTED)			
DECIMAL ±		SCALE 1/2	DRAWN BY T. RYAN
			APPROVED BY
FRACTIONAL ±	TITLE EARTHQUAKE STUDY PHANTOM		
ANGULAR ±	DATE 4-7-82	DRAWING NUMBER 00011-82-C-00	

K•E ALBANENE ® 10 5466 ENGINEERS' STANDARD FORM

MADE IN U.S.A.

FIGURE 6

Each tomogram described displays a gray scale on the left and "ruler" marks on the right, along with pertinent details on the tomographic parameters used in the reconstruction procedure (e.g. grid size, pixel size, etc.). On the gray scale used, the brighter regions correspond to the higher density and the lower densities appear as darker regions on the tomogram. Tomograms are normalized so as to display the true mass density distributions.

Without going into great detail we wish to mention that the "raw" transmission data collected during any particular examination were subjected to a variety of data smoothing, filtering and noise reduction techniques via extensive software developed by SMS, Inc. over the past six years. In this fashion we have been able to suppress and/or entirely remove a number of artifacts usually encumbering the tomographic data. Since it is beyond the scope of Phase I of this research, we have not delved into the question of the enhancement of the image quality, in a greater detail than mentioned earlier. The issue of obtaining the best image quality in itself would constitute a pertinent subject for extensive research.

(1) Collimation study. In the series of tomographic examinations conducted, the effective source dimensions were 3.00 mm x 3.00 mm. The 50 Ci ^{60}Co source is in a cylindrical pellet shape with the top end shining at the object. The detector bank has two collimation apertures available. One being 2.00 mm x 2.4 mm and the other one being 20.0 mm x 6.4 mm; implying a significantly fine slice volume sampled in the former case. The use of wide aperture leads to higher transmission count rates and consequently better statistics but it also adds to the noise arising from the scattered radiation. This effect is clearly observed.

The entire study on the influence of collimation was conducted comprehensively, using 640 viewing angles and 462 rays in the photon fan beam. This

corresponds to a ray spacing of 1.167 mm at halfway between the source and the detector bank. It should be noted that the spatial resolution attainable in a tomographic scan is ultimately limited by the geometry of the setup, i. e., the ray spacings or the extent of the sampling.

Tomogram #1: A tomogram of a cross-section of the entire phantom is displayed in Fig. 7 and corresponds to a collimation of 2.4 mm and 640 angular views with 1.167 mm ray spacings at the center. The grid size for the display is 128 x 128 and correspondingly the pixel size is 3.77 mm x 3.77 mm. Since the pixel size is relatively large, a detail in the cross-section of an extent smaller than this, does not afford a clear visual discrimination. This is evident from the section of the tomogram (lower left corner) containing the 1/8" aluminum pipes. However, it should be noted that the lack of clear visual distinction does not necessarily imply a poor resolution of the features, as will be shown later in the tomogram displaying only the section of the fine details.

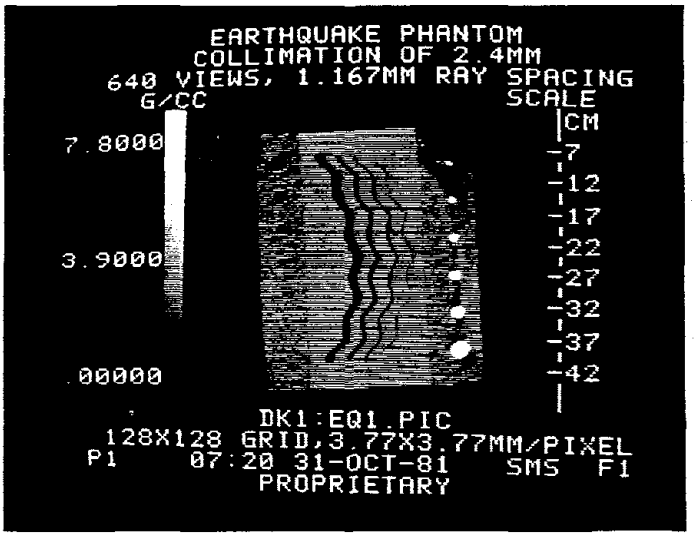

Fig. 7

All other features of the phantom, the aluminum cylinders, the cracks, the rebars and the distinction between the aggregate-sand composition and the concrete block are well resolved. The upper right hand corner clearly displays the lack of aggregate-sand background, where the level of the aggregate-sand background inadvertently fell below the probe beam height.

Tomogram #2: In Fig. 8 we show the tomogram displaying the section of Tomogram #1, containing the two 1/8" and the 1/4" inner diameter aluminum pipes. The reconstruction of this section was done using the entire data set and the display is on a 64 x 64 grid with the pixel dimension of 1.18 mm x 1.18 mm . As mentioned earlier, display on a finer pixel size indeed exhibits the good resolution of the finer details. The aggregate-sand background is visually well resolved. The aluminum cylinder composing the 1/4" void is also well discriminated with respect to the background.

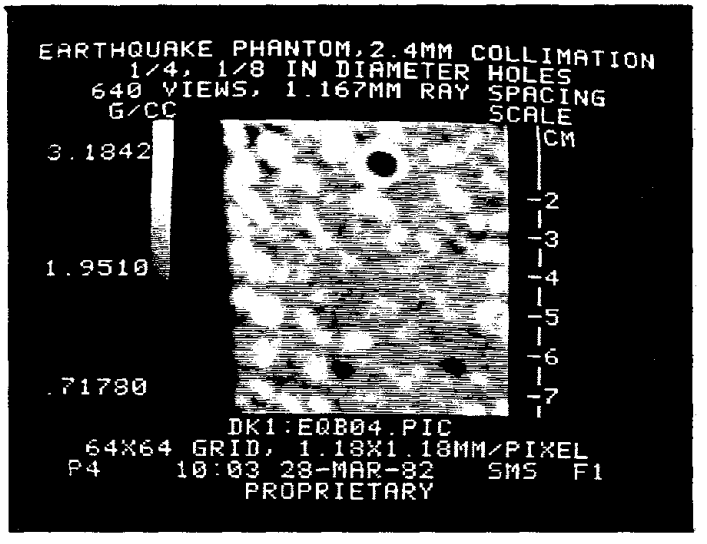

Fig. 8

Such a "blown-up" reconstruction of any section of interest of a tomogram is quite readily obtained once the initial set of data is processed and requires less than 10 minutes (CPU time) on the SMS PDP-11/35 system. The display software is capable of demarking any desired density range, making possible a rapid comparative examination of the tomogram for the variation and distribution of the mass densities contained.

Tomogram #3: The tomogram displayed in Fig. 9 corresponds to a collimation of 6.4 mm, with all other parameters fixed to be the same as in Tomogram #1. (Please note that the aggregate-sand mixture was repacked to remove the air-gap displayed in Tomogram #1.) All of the fine details are clearly visible and well resolved as in Tomogram #1, except for the case of the 1/8" inner diameter aluminum pipes. The "smearing" effect due to the larger aperture size is evident for this section of the tomogram, although its effect is imperceptible for the remaining region of the object cross-section. There are circular artifacts present in this tomogram, attributed to the increased level of the scattered radiation. Although difficult for an untrained eye to observe these artifacts, their presence is clearly observed in the "blown-up" reconstruction displayed in the next tomogram.

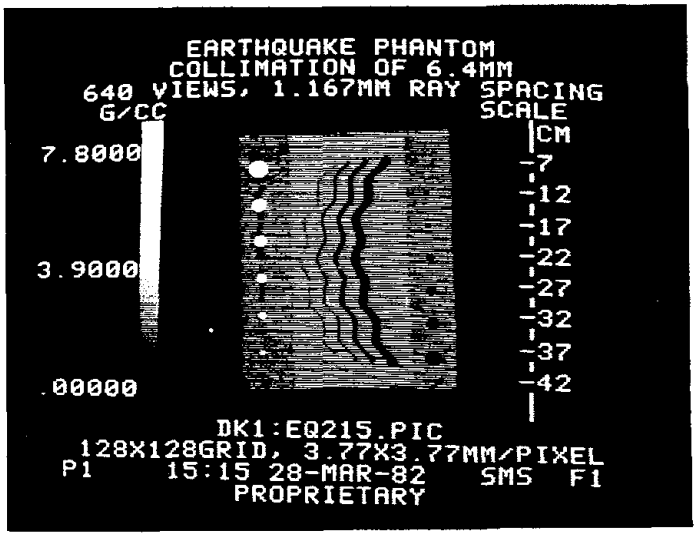

Fig. 9

Tomogram #4: Figure 10 displays the reconstruction of the phantom section described in Tomogram #2. The circular artifacts are now clearly visible in contrast to the display in Figure 9. Also the fact that the fine features of this section are resolved is quite evident. The presence of the artifacts, in this case, does not deteriorate substantially the degree of resolution and hence no further effort was made to completely remove these artifacts. A "streak" artifact present in the lower left region of the tomogram is an artifact arising out of one erroneous data point during any one angular position. Such errors are readily removable. However, unless they tend to shadow a feature of interest their removal is not implemented. The influence of the lesser degree of collimation is exhibited in the "smeared" contrast for the background, where the structure is not as well discriminated as in Tomogram #2. This is due to the fact that a 6.4 mm collimation at the detector corresponds to $\sim$ 3.2 mm sampling extent at the center. The increased sampling size leads to the smearing of the image and hence the consequent lack of contrast in the display.

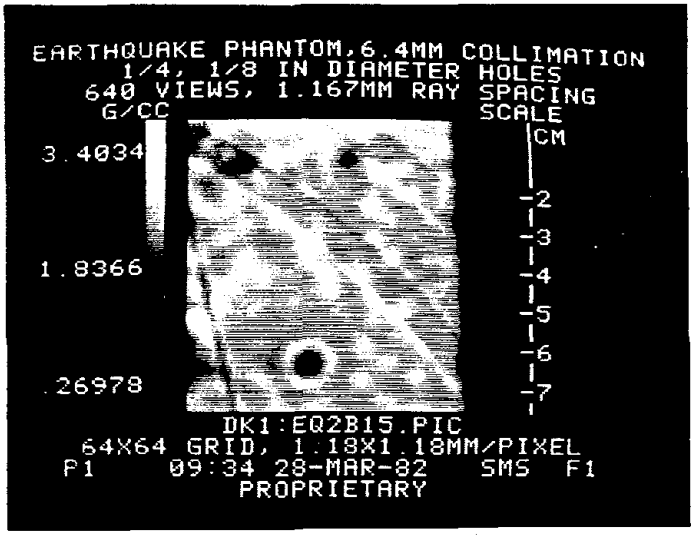

Fig. 10

(2) Limited view examination. For the two cases of collimation described above, a study was conducted to investigate the resolution attainable of the phantom details for the limited view tomographic examination. When an object is of such physical extent as to prohibit the necessary 360^{o} access, (e. g. a wall), the use of tomographic process would lead to only a partial collection of the information. We have examined two specific cases for this study. In one case a 135^{o} viewing range was selected and in the second case the viewing range was limited to 90^{o}. The views were taken symmetrically from the longer side of the phantom. The ray spacing was kept at 1.167 mm for both these cases and scans were repeated for a 6.4 mm collimation aperture.

Tomogram #5: Figure 11 displays a 135^{o} partial view scan tomogram with a collimation of 2.4 mm. Due to their circular symmetry the rebars and the aluminum pipes afford a better degree of visual detection as compared to the cracks. If the viewing range is such that at least one ray passes parallel through a crack section, then that portion of the crack is better demarked. This fact is displayed in the tomogram where the presence of voids is evident. It should be noted that although the presence of an anomaly is detected, it does not afford a sound basis for interpretation and/or evaluation. This is obvious since we are dealing with only a limited set of information.

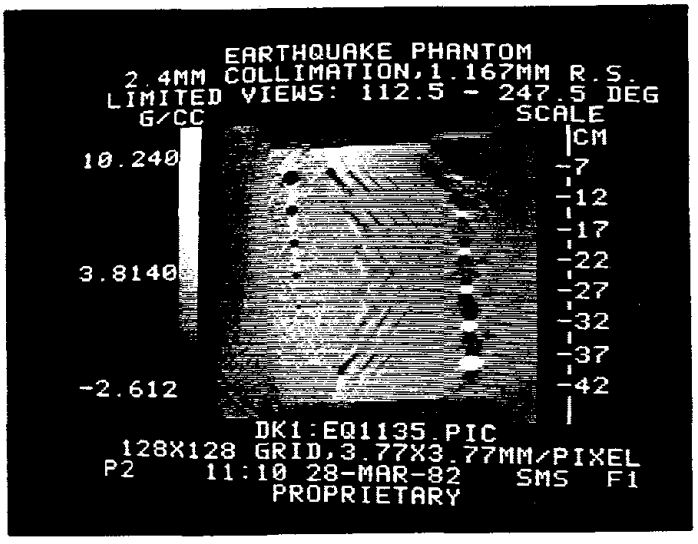

Figure 11

Tomogram #6: Figure 12 displays a partial view scan with a viewing range of 90°. All other parameters are the same as for Tomogram #5. A further reduction in the definition of the cracks is clearly exhibited.

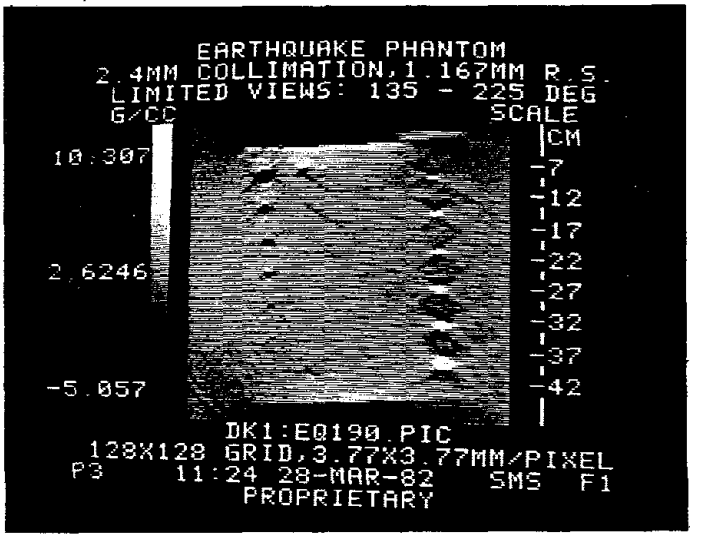

Fig. 12

Tomograms #7 and #8: In Figures 13 and 14 the situations corresponding to Tomograms #5 and #6 are re-examined with a wider collimation aperture of 6.4 mm. The marked difference between the two collimation selections is shown by the absence of detail on the aggregate-sand background when a 6.4 mm collimation aperture is used. The smearing effect causes a degraded resolution and only the areas containing a large density contrast (steel and background or air and background) tend to show up.

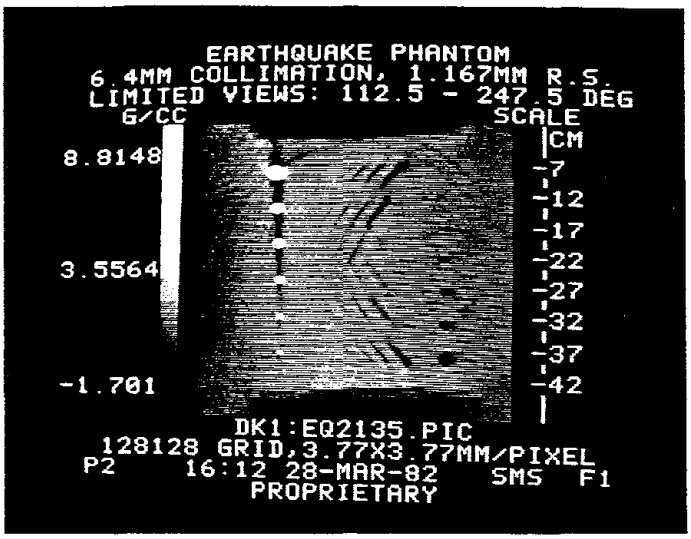
EARTHQUAKE PHANTOM
6.4MM COLLIMATION, 1.167MM R.S.
LIMITED VIEWS: 112.5 - 247.5 DEG
G/CC
SCALE
CM
8.8148
3.5564
-1.701
-7
-12
-17
-22
-27
-32
-37
-42
DK1:EQ2135.PIC
128128 GRID,3.77X3.77MM/PIXEL
P2 16:12 28-MAR-82 SMS F1
PROPRIETARY

Fig. 13

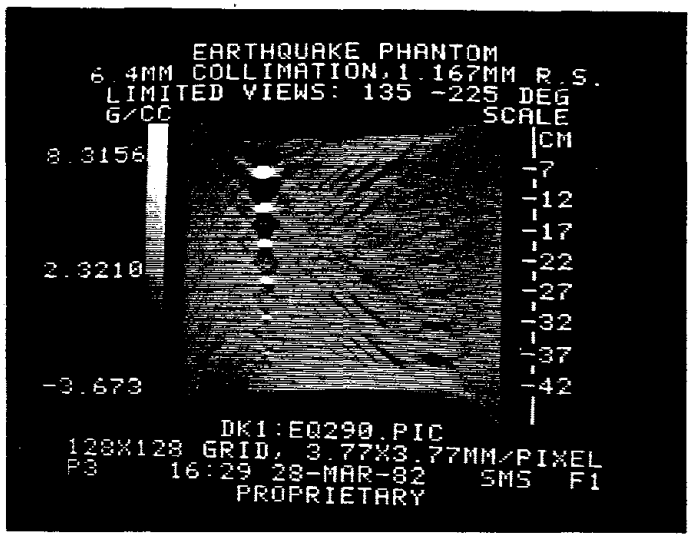
EARTHQUAKE PHANTOM
6.4MM COLLIMATION,1.167MM R.S.
LIMITED VIEWS: 135 -225 DEG
G/CC
SCALE
CM
8.3156
2.3210
-3.673
-7
-12
-17
-22
-27
-32
-37
-42
DK1:EQ290.PIC
128X128 GRID, 3.77X3.77MM/PIXEL
P3 16:29 28-MAR-82 SMS F1
PROPRIETARY

Fig. 14

Before continuing with the description of the rest of the tomograms, we wish to point out that although there is an obvious lack of information for a limited view scan, it has the advantage of rapidly distinguishing features of high density contrast and/or features of sufficiently large dimensions. Also it should be pointed out that in processing the partial set of data, no a priori information about the object, such as the geometrical shape, was used. Use of such additional a priori information about the object can be very useful in interpreting the data obtained, and a limited view tomographic examination would provide a useful and rapid NDT/NDE technique.

(3) Study of angular positions and the ray spacings. The concluding part of the tomographic examination consists of studying the influence of the varying number of angular views and the size of ray spacings on the spatial resolution attainable. Both the number of angular views and the ray spacings are equally important in determining the degree of spatial resolution. Also the total time required for any complete tomographic scan depends linearly on the number of ray paths and angular views.

The influence of these parameters on the image quality is well portrayed in Tomograms #9 to #17, shown sequentially in Figures 15 through 23. Figures 15 through 17 are the tomograms reconstructed for 640 views and the ray spacings of 1.167 mm, 4.668 mm and 9.336 mm, respectively. The effect of increasing the sampling size is quite clearly exhibited with features of extent 4.6 mm and less being either poorly resolved or totally unresolved. The entire set of tomograms for this study was conducted with a 6.4 mm collimation aperture. As discussed earlier, this contributes to the added noise through the scattered radiation. The circular artifacts arising from this are more pronounced for the case where the sampling dimension is increased. With the ray spacing of 9.336 mm the two smallest cracks are very poorly resolved due to the magnitude of the sampling extent.

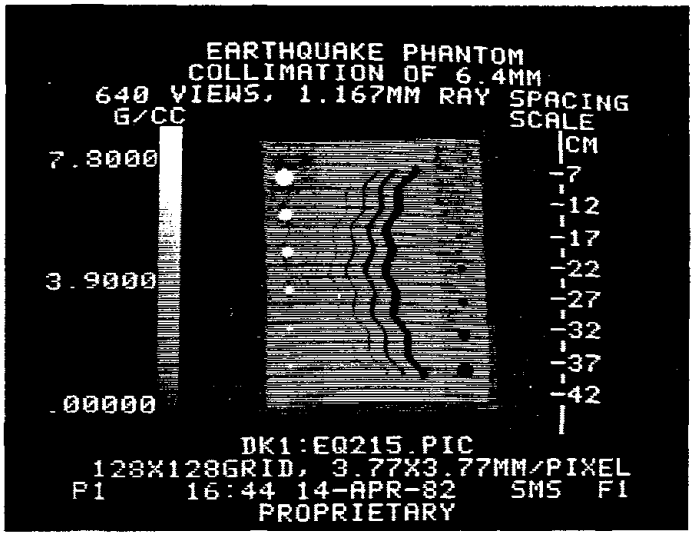

Fig. 15

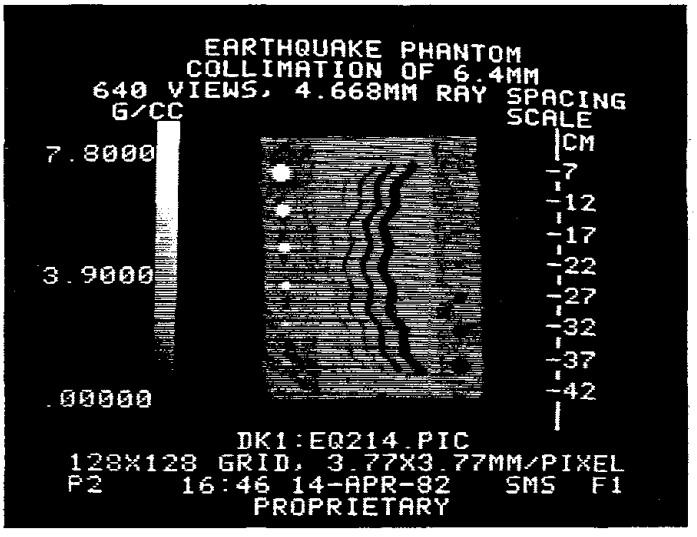

Fig. 16

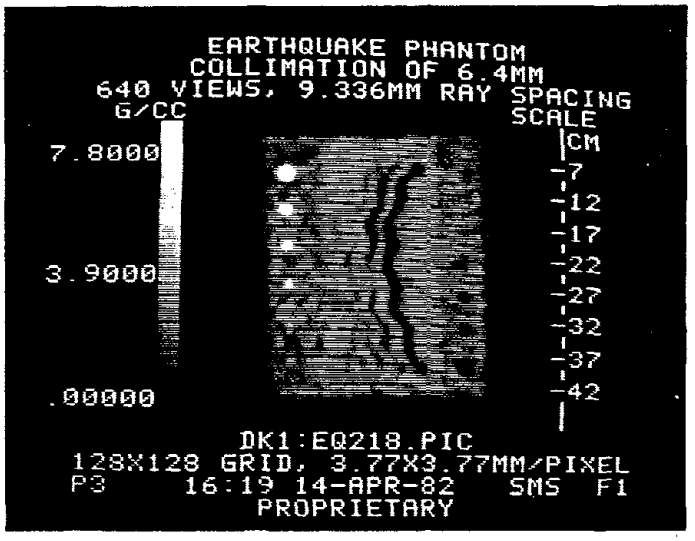

Fig. 17

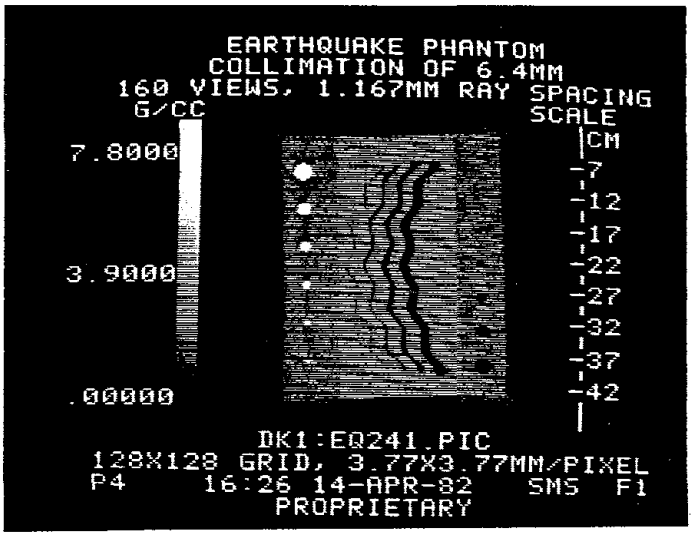

Fig. 18

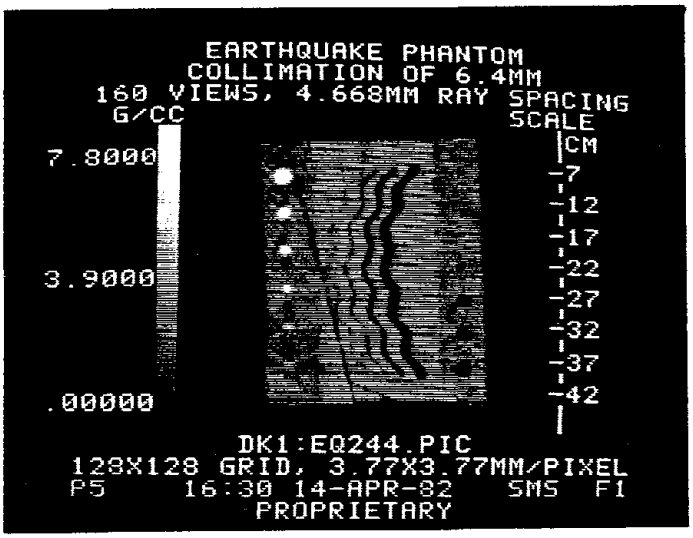

Fig. 19

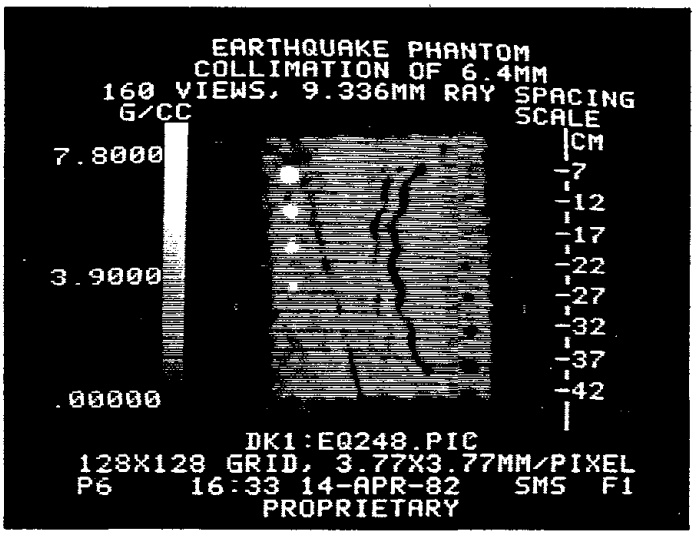

Fig. 20

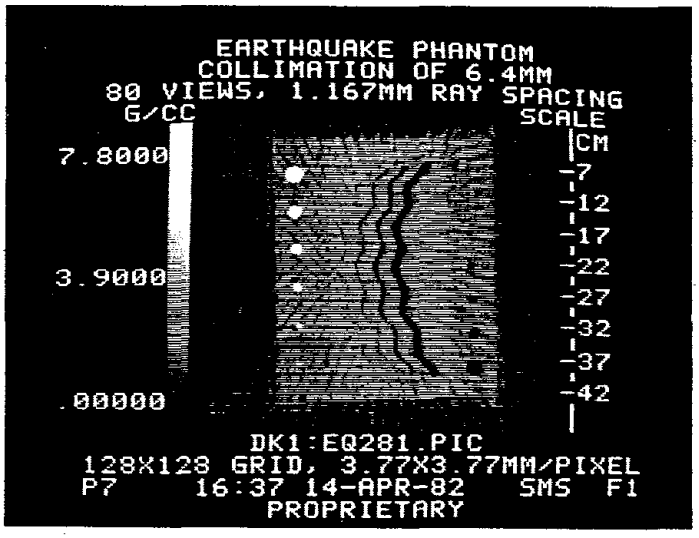

Fig. 21

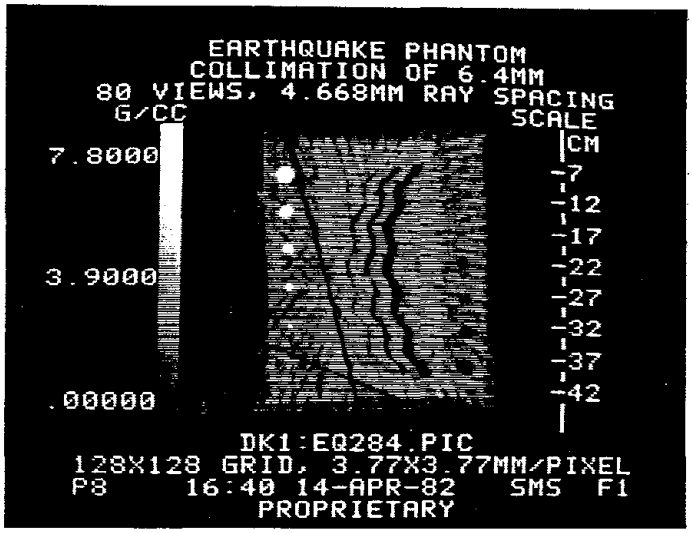

Fig. 22

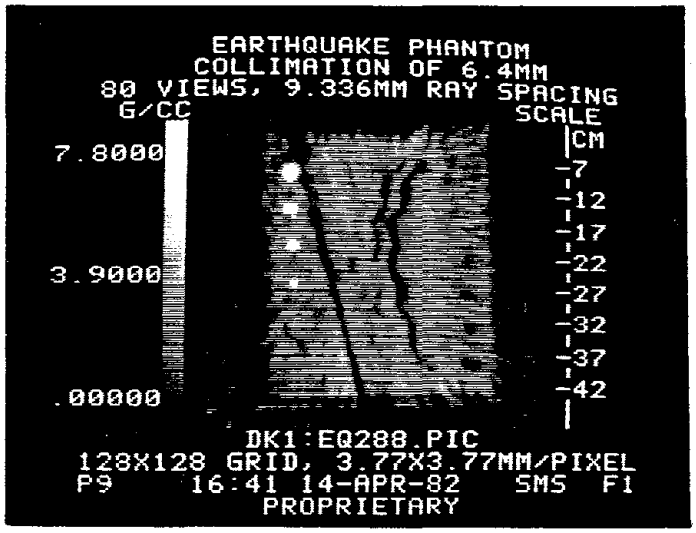

Fig. 23

The use of a large sampling extent essentially causes an averaging of the mass distribution contained within the sampling region, i.e., a smearing of the density is produced. In Tomogram #11 this smearing effect causes the concrete block boundary to be poorly defined. The rebars are still visually detectable simply because the density contrast between steel (7.87 g/cc) and the background average $\sim$3.0 g/cc) is considerably larger than between the concrete block and the background. Tomograms #12 through #14, shown in Figures 18 to 20, correspond to the same variation in the ray spacings as before but with one-fourth as many views (i.e. 160 views). Effects of the reduced number of views are obvious in comparison with the previous three tomograms. The visual contrast showing the background "graininess" is significantly marred due to the "streaks" which are typical of a scan taken with relatively fewer angular views. This effect, i.e. the influence of the number of views on the quality of the image and consequently on the resolution attainable is even more clearly marked in the last set of tomograms #15 to #17, shown in Figures 21 through 23. The line artifact, which is weighted down when the number of views and the number of rays are larger, is now more prominent and becomes broader as the ray spacings increase.

Decreased number of views and/or increased ray spacings correspond to an undersampled situation. The set of nine tomograms described above shows clearly the trend of degradation in spatial resolution as a function of these parameters. However, it is very clear that if the features of interest pose a sufficient density contrast relative to the background and/or their dimensions are amenable to a coarse sampling, a substantial reduction in the angular views and the ray spacings is permissible. Consequently the scanning as well as the processing time can be reduced substantially. This may be illustrated

by comparing approximately 10 hours required for the production of Tomogram #9 to approximately 1 hour required for the case in Tomogram #17. A priori knowledge of the characteristics of features is thus useful in determining the values of the pertinent tomographic parameters.

(c) Compton Interaction Tomography

As described in Section 2, the Compton Interaction Tomography (CIT) is based on measuring the electron density distribution in an object through the measurement of the backscattered intensity. Feasibility of CIT technique for NDT/NDE of an extended object was checked experimentally on the special aparatus setup, described in Section 3. In this subsection we discuss the experiment and the results obtained. The results of the experiment depend very sensitively upon a number of crucial parameters. These are essentially the source and detector characteristics, the degree of collimation, and the source-detector geometry. We discuss below the significance and influence of these parameters.

(1) Geometry. As shown in Fig. 3, the source-detector geometry is essentially controlled by the scattering angle, φ, chosen for a backscatter study. The geometry of the setup plays an important role, in that it determines the path lengths and hence the magnitude of the linear attenuation experienced by the photon beam. It also determines the shape and the size of the focal volume, which controls the signal strength and differential averaging effect on the backscattered signal, as explained later. Let us consider the effect of attenuation first. The backscattered photon energies depend on the scattering angle. However, the intensity of the backscattered signal, apart from its dependence on the scattering angle, depends also upon the net linear attenuation suffered by the beam during its passage through the medium.

The total attenuation depends not only on the path lengths but also upon the photon energies. In the Compton backscatter study there are two

photon energies and hence two different μ values involved, one for the incident beam and the other for the backscattered beam. For a fixed scattering angle, the individual path lengths for the incident and the scattered photon beams depend on the source inclination angle, θ_1, and the detector inclination angle, θ_2. Since the scattered photon energies are less than the incident photon energy, the attenuation coefficient, μ_{sc}, for the scattered beam is larger. Consequently, to maximize the output signal, θ_1 needs to be larger than θ_2. Theoretical calculations for θ_1, over a range of scattering angles are given in Table 1, for a ^{60}Co source and in Table 2, for a ^{137}Cs source. Calculations are included in these tables for the Compton cross-sections, i.e., the probability that an incident photon will scatter off an electron in the focal volume at a given angle, φ. The selection of the scattering angle, apart from the consideration of the attneuation, is also influenced by the detector characteristics discussed later.

Returning now to the question of the geometry of the focal volume, the most important point is that of differential averaging. The focal volume is defined by the source and the detector collimations. For a given focal volume, defined by the setup of the experiment, the backscattered signal depends on the electron density contained within the focal volume. If more than one medium is intersected by the focal volume, the signal strength reflects the average value of the electron density contained within this volume. Thus as the focal volume probes across a bounary separating two media, the change in the signal varies gradually in proportion to the fraction of the focal volume contained in each medium. This variation in the signal across a boundary, termed as differential averaging, leads to a "smoothing" of the edge. This is, therefore, of importance in interpreting the data for the location of the boundary.

TABLE I

Source: ^{60}Co Incident Energy 1250.0 keV

Medium: Concrete $\rho = 2.3$ $Z = 9.4$ $A = 18.7$

Scattered Energy (keV)	Scattering Angle, φ	Source Inclination (deg) θ_1	Compton Cross Section (10^{-25})
1249.53	1.00	89.54	0.70340
1196.24	11.00	84.54	0.71474
1075.29	21.00	79.76	0.55658
926.34	31.00	75.10	0.39800
781.24	41.00	70.65	0.27833
655.56	51.00	66.42	0.19955
553.04	61.00	62.29	0.15060
471.74	71.00	58.19	0.12063
408.03	81.00	54.07	0.10215
358.28	91.00	49.87	0.09055
319.45	101.00	45.54	0.08311
289.16	111.00	40.95	0.07825
265.61	121.00	36.08	0.07501
247.47	131.00	30.84	0.07283
233.77	141.00	25.19	0.07135
223.79	151.00	19.16	0.07037
217.05	161.00	12.76	0.06975
213.23	171.00	6.10	0.06942

TABLE II

Source: ^{137}Cs Incident Energy: 662 keV

Medium: Concrete $\rho = 2.3$ $Z = 9.4$ $A = 18.7$

Scattered Energy (keV)	Scattering Angle, φ	Source Inclination (deg) θ_1	Compton Cross Section ($X10^{-25}$)
659.87	1.00	89.54	.79368
644.70	11.00	84.54	.74414
607.85	21.00	79.61	.63262
557.21	31.00	74.82	.49907
501.21	41.00	70.12	.37686
446.32	51.00	65.57	.28163
396.29	61.00	61.05	.21486
352.74	71.00	56.64	.17143
315.86	81.00	52.24	.14483
285.20	91.00	47.81	.12950
260.04	101.00	43.26	.12133
239.61	111.00	38.60	.11754
223.21	121.00	33.73	.11627
210.26	131.00	28.62	.11638
200.28	141.00	23.26	.11711
192.91	151.00	17.59	.11799
187.88	161.00	11.68	.11878
185.02	171.00	5.58	.11929

The size of the focal volume, in the direction of probing becomes an important consideration when the anamoly to be detected (e.g. air voids or cracks in concrete) is of an extent smaller than the focal volume dimensions. The smoothing of the edges in such cases can substantially hinder an accurate interpretation. It is obvious from simple geometrical considerations that as the source-detector angle (i.e. $\theta_1 + \theta_2$) increases, the extent of the focal volume in the direction perpendicular to the source-detector line decreases, and consequently the differential averaging effects are less pronounced. Although a decreased smoothing permits a finer demarcation of an edge, this case also implies a decreased scattering angle and for the reasons explained later, it could hinder a clear detection. Conversely, a smaller source-detector angle would lead to an increased degree of smoothing. Thus there is a considerable interplay between the conditions for the optimization of the output signal and the effects produced by the differential averaging. In addition the characteristics of the feature to be detected, such as its orientation and extent, also influence the selection of the geometrical parameters.

The experimental study to investigate the feasibility of the CIT process was supplemented by a simulation study. The theoretical considerations on attenuation are already mentioned earlier. The differential averaging effect was studied for several different focal volume extents. This is explained later when we study the trends of the backscattered signal intensities with different target media. For the present, as an example of the differential smoothing, we consider the situation depicted in Fig. 26. A steel plate of 0.5" thickness was probed with a ^{192}Ir source. The source and the detector inclinations were chosen to be 45° each, implying a backscattering angle of 90°. The backscattered signal, in terms of counts/sec is plotted against the

depth probed. The initial rise in the signal is due to the increase of the focal volume intercepted by the plate and the later drop is as it proceeds past the plate. Such a scan can be used for determining the extent of the focal volume from the knowledge of the true dimension of the object. From this particular test, the focal volume extent for the experimental setup was determined to be of ~25 mm along the probe direction.

(2) Collimation. The influence of collimation of the source and the detector on the focal volume is obvious. The main advantage of collimation of the detector is in suppressing the multiply scattered photon signal which contributes to the noise. The signal of interest corresponds to singly scattered photons from the target volume received at the detector. However, the photons in the incident beam can undergo multiple scattering off any point within the object such that it may be received at the detector. Such multiply scattered photons contribute to the low energy end of the backscattered spectra. Fine collimation tends to minimize such contributions. However, it should be noted that too fine a collimation would also tend to reduce the intensity of the singly scattered (or the "primary" scattered) beam.

(3) Source and detector characteristics. The important source characteristics are the intensity of photon flux and the photon energies. Isotopic radioactive sources may emit photons predominantly at one frequency or may possess several groups of frequencies in its emission spectrum. Both the photon energies and the flux strength are important in the backscatter studies. Higher photon energies can penetrate greater depths in a medium since the attenuation coefficient tends to decrease at higher energies. On the other hand, the probability for a primary scattering to take place (i.e. the Compton interaction cross-section) also tends to decrease with the increased photon energies.

The flux strength of the source has obvious importance since the intensity of the backscattered signal is directly proportional to the incident flux. When the source emissions are at more than one photon energy, i.e. if the source is not monochromatic, there is a further increase in the range of energies of the multiply scattered photon background. On the other hand, the polychromaticity of a source can be used to an advantage by using different energy discriminations at the detector. The lower energy spectral components can be used for probing relatively short depths of a medium whereas the higher energy components may be used for probing greater depths.

One more consideration pertinent in the selection of sources is what is termed as the gamma multiplicity and represents the average number of photons emitted per disintegration. ^{60}Co source, for example, has a multiplicity of 2.0. It is 2.3 for ^{192}Ir and 0.8 for ^{137}Cs. Together with the photon energies, the gamma multiplicities dictate the choice of the sources.

A simulation study to investigate different sources is shown in Fig. 27, where 100% detection probability has been assumed for all photon energies. The backscatter detection probability per incident photon is plotted as a function of the depth in the medium. The situation chosen corresponds to a 0.5" steel plate embedded 4" from the front surface of a concrete block. The photon sources chosen were ^{60}Co, ^{192}Ir and ^{137}Cs. ^{60}Co has predominant photon emissions around an average energy of 1250 keV, whereas ^{192}Ir spectrum has three groups around 310 keV, 468 keV and 610 keV. The relative strengths of the ^{192}Ir groups are 68%, 23% and 8% respectively. ^{137}Cs has a single emission at 662 keV. The 468 keV line of ^{192} Ir was used for the simulation study. The backscatter angle selected was 90^{o} and the focal volume had a 10 mm extent along the direction of probing. At 90^{o} scattering angle, the backscattered photon energies

are 363 keV, 244 keV and 288 keV for the ^{60}Co, ^{192}Ir and ^{137}Cs sources respectively. The ^{60}Co source clearly yields the greatest relative backscatter signal from the steel. However, at depths less than 4", the ^{192}Ir and ^{137}Cs provide comparable or greater signals.

It should be pointed out that the backscatter probability in Figure 27 is per incident photon. Hence, in order to estimate the backscatter intensity obtainable in a given situation, the total source yield must be considered. The source yield is a product of the activity of a particular volume, reduced by any self-absorption which occurs, and the gamma ray multiplicity for a specific gamma ray line or group of lines of interest. Based on practical limitation in fabrication, nominal total specific activities are ~ 17, ~ 3, and ~ 0.1 Curies per mm^3 of ^{192}Ir, ^{60}Co, and ^{137}Cs, respectively.

Folding in the gamma ray multiplicities and self-absorption effects with the specific activities yields maximum intensities of $\sim 5 \times 10^{11}$ photons/steradian-sec, $\sim 10^{11}$ photons/steradian-sec, and $\sim 10^{8}$ photon/steradian-sec from each mm^2 area of ^{192}Ir, ^{60}Co, and ^{137}Cs, respectively. Strengths of 200 Curies of the first two sources are readily available commercially, with source dimension on the order of 3-10 mm. Greater intensities, up to several thousand Curies can also be obtained. In general, either ^{192}Ir or ^{60}Co will suffice for almost any application where photons in the energy range of 300-1300 keV are needed.

Other practical considerations influencing source selection include signal-to-multiple scattering characteristics, shielding requirements, availability, size and cost. The first of these is very difficult to estimate accurately and is best gauged by making relevant empirical measurements of the type presented in this report. The later logistical factors are well known. Two hundred Curies of ^{192}Ir is used in a 35 - 40 lb exposure device meeting

National Regulatory Commission and the Department of Transportation specifications for shipping and safe use, with a total cost of $\sim$ \$5,000 to \$7,000 per system. Two hundred Curies of ^{60}Co resides in a 350 - 500 lb. device which costs \$15,000 to \$25,000, including the source. The short half-life of ^{192}Ir, 74 days, requires frequent source capsule changes ($\sim$\$1,500) to maintain reasonable intensities, whereas the 5.3 year half-life of ^{60}Co -- makes a single source useable for several years.

Returning to Fig. 27, the initial rise in the probability is due to the increase in the fraction of the focal volume as it gradually enters the concrete medium. The later linear drop represents the characteristic exponential attenuation in the radiation beam as it propagates through the medium. As the focal volume encounters the steel plate, the differential average effect is evident. The rise in the probability at this location is due to the increased electron density encountered. Once the focal volume sweeps past the steel plate, the decrease in probability is a combined effect of an overall increased attenuation (due to both the presence of steel plate as well as increased path lengths) and the decrease in electron density.

As far as the detection system goes, the choice of detector depends on the type of radiation to be detected. For gamma radiation, NaI crystal scintillation detectors and semiconductors, such as Geli, are most commonly used. The parameters of significance for characterizing such detectors are the active volume of the crystal and the resolution at a given energy. The active volume of the crystal controls the fraction of the incoming energy absorbed and hence is a measure of the efficiency of the detector. Resolution of the detector is important in clearly distinguishing group frequencies. For the case of the NaI crystal used for the present experimental study, the

cylindrical crystal dimensions of 1.5" diameter and 1.5" length provided sufficient volume for a complete absorption in the energy range of interest, (242 keV - 295 keV). The resolution of the crystal was measured to be 26% at 186 keV, using a ^{226}Ra calibration source.

With these preliminary considerations we proceed to discuss the details of various experiments performed. All of the experiments were conducted with a 25 Ci, ^{192}Ir source. The spectral components of this source have been discussed earlier. For the detector system a cylindrical NaI crystal of 1.5" diameter and 1.5" length was used with a photoelectric tube voltage at 1400 volts. The amplified output of the phototube was analyzed through a LeCroy QVt multichannel pulse-height analyzer. The detector was calibrated using a ^{226}Ra source. For the entire series of experiments the scattering angle was chosen to be of 90° and the source inclination angle was kept at 45°. The source shielding constituted approximately 6" of lead. In addition, an 8" x 4" x 4" lead block with a 1 cm x 1 cm hole through it was installed in the front of the source to collimate the incident beam. An identical lead block collimator was used for the NaI detector. Prior to the calibration stage, measurements were made for determining the net background signal with the detector aperture blocked. This background signal constitutes the total noise present in the system, from the stray radiation through all the shielding, the noise in the detection system electronics, etc. Since the scattering angle was 90°, the backscattered signal is composed of photon groups at central energies of 178 keV, 244 keV and 278 keV for the ^{192}Ir source used. Although the 310 keV photon group of Iridium constitutes 68% of the source emissions, the backscattered signal (at 178 keV) is quickly lost in concrete. The backscattered spectra for a uniform concrete medium from the depths of 2.5 cm and 7.5 cm are shown in Figs. 25(a) and 25(b). The loss of 178 keV line within

the background noise at 7.5 cm is quite evident. NaI crystal does not possess a very sharp resolution. At 186 keV the resolution is $\sim$ 26%, i.e. the full width at the half maximum of the pulse centered around 180 keV line is $\sim$ 47 keV wide. It is due to this resolution characteristics that the 244 keV and 278 keV groups in the backscattered spectra are not individually resolved. For this reason the energy window in the multichannel analyzer was selected to cover the range of 242 keV - 295 keV.

Experimental Studies:

To investigate the feasibility of the CIT processes as NDT/NDE techniques a study was conducted to detect the presence of iron rebars and air voids located in a concrete background medium. In the remainder of this subsection we describe various experiments performed and the results obtained.

(i) The first set of experiments performed was for determining the character of the backscattered spectra and hence for determining the necessary energy window. The backscattered spectra from a concrete block were obtained for the depths of 2.5 cm and 7.5 cm, respectively. The plots of the backscattered counts as a function of the energy are shown for these two cases in Figs. 24(a) and 24(b), respectively. The backscattered portion of the incident 310 keV photon group is rapidly dominated by the background noise as the depth increases. The 468 keV and 610 keV incident photon groups yield a backscattered signal which is still separable at greater depths. For this reason, the energy window (or the energy gate) was selected to be from 242 keV to 295 keV.

After the energy window selection, an experiment was performed for determining the backscattered signal strength as a function of the depth in a concrete medium without any other objects embedded in it. The variation in the signal strength as a function of the depth in medium is shown in Fig. 25. The initial rise in the signal is due to the differential averaging as the focal volume

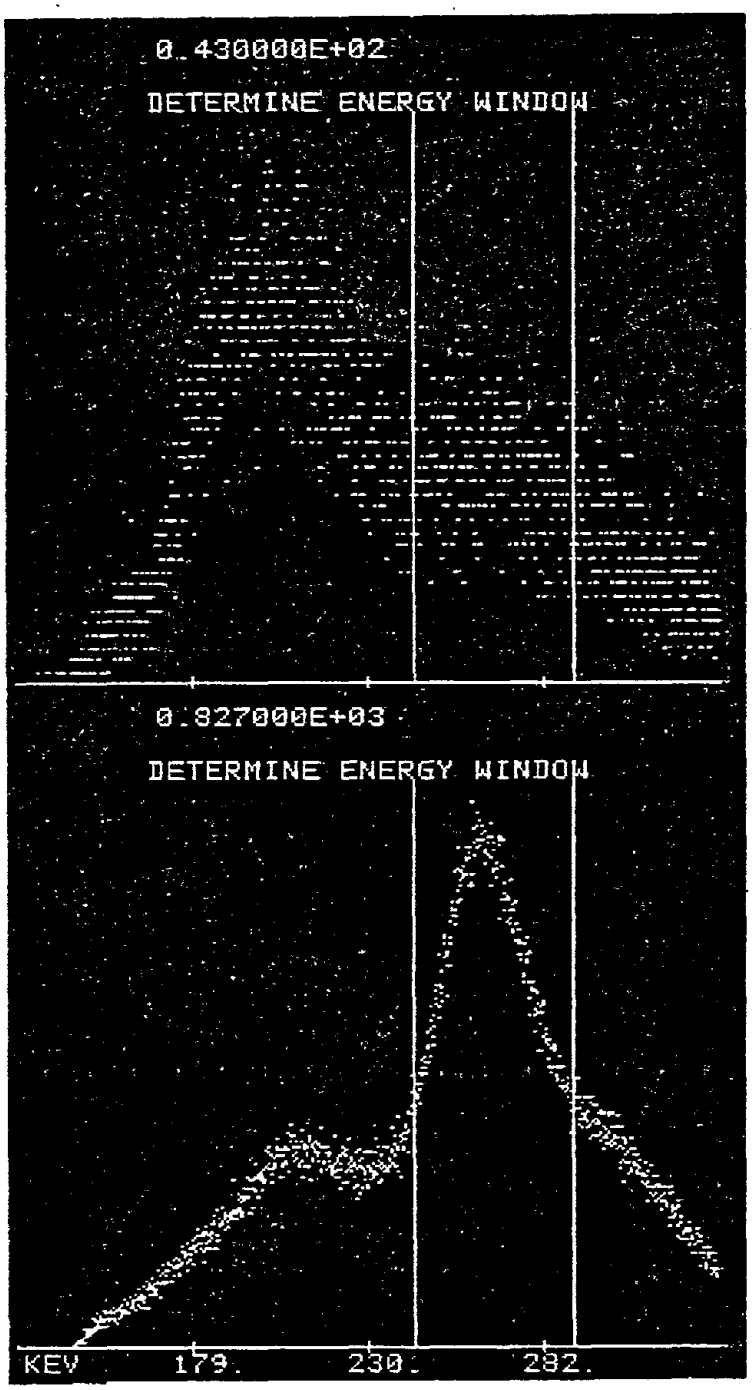

Fig. 24a. Backscatter spectrum 7/5 cm into block (lines indicate energy gate).

Fig. 24b. Backscatter spectrum 2.5 cm into block.

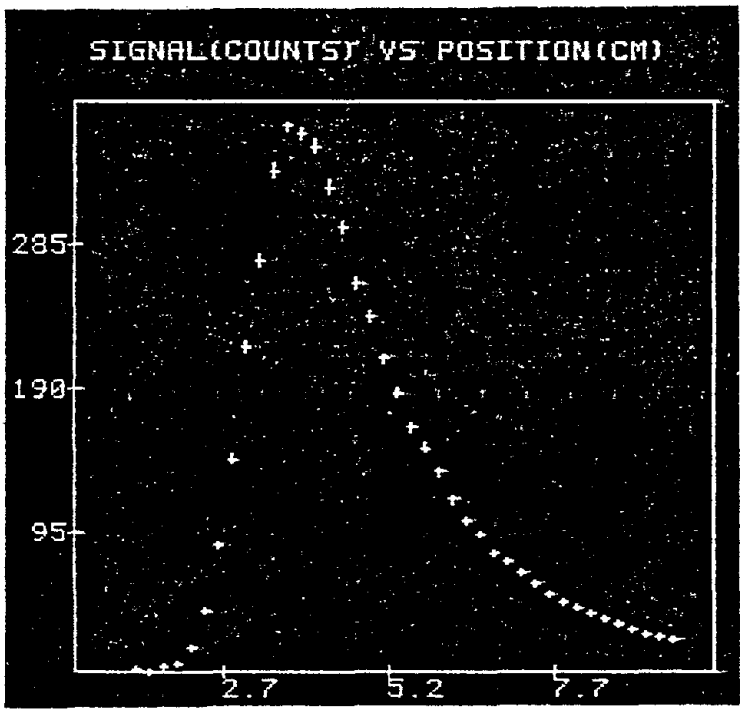

Figure 25

Backscattered signal from a concrete medium

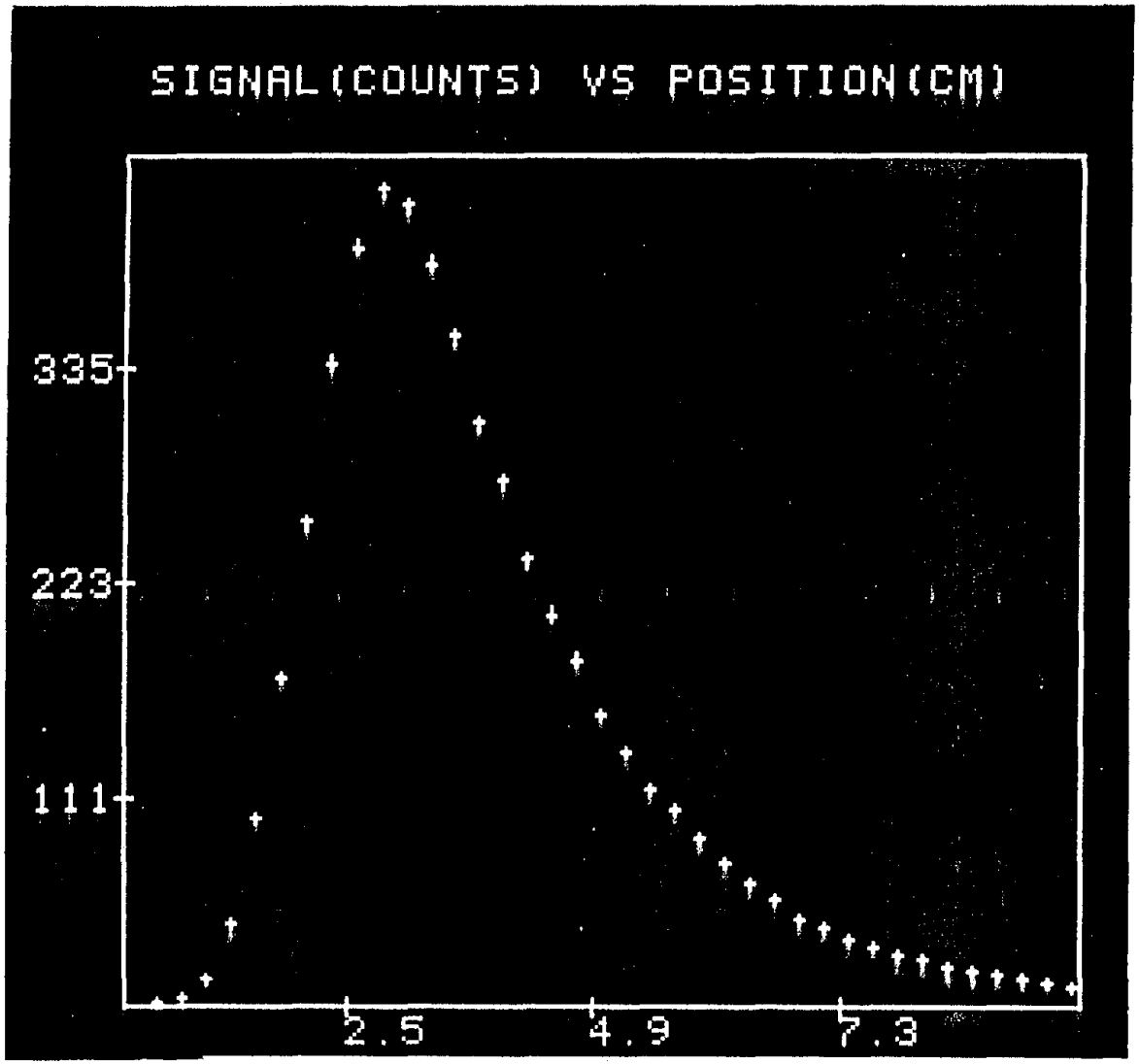

FIGURE 26.

Backscattered signal from 0.5" steel plate

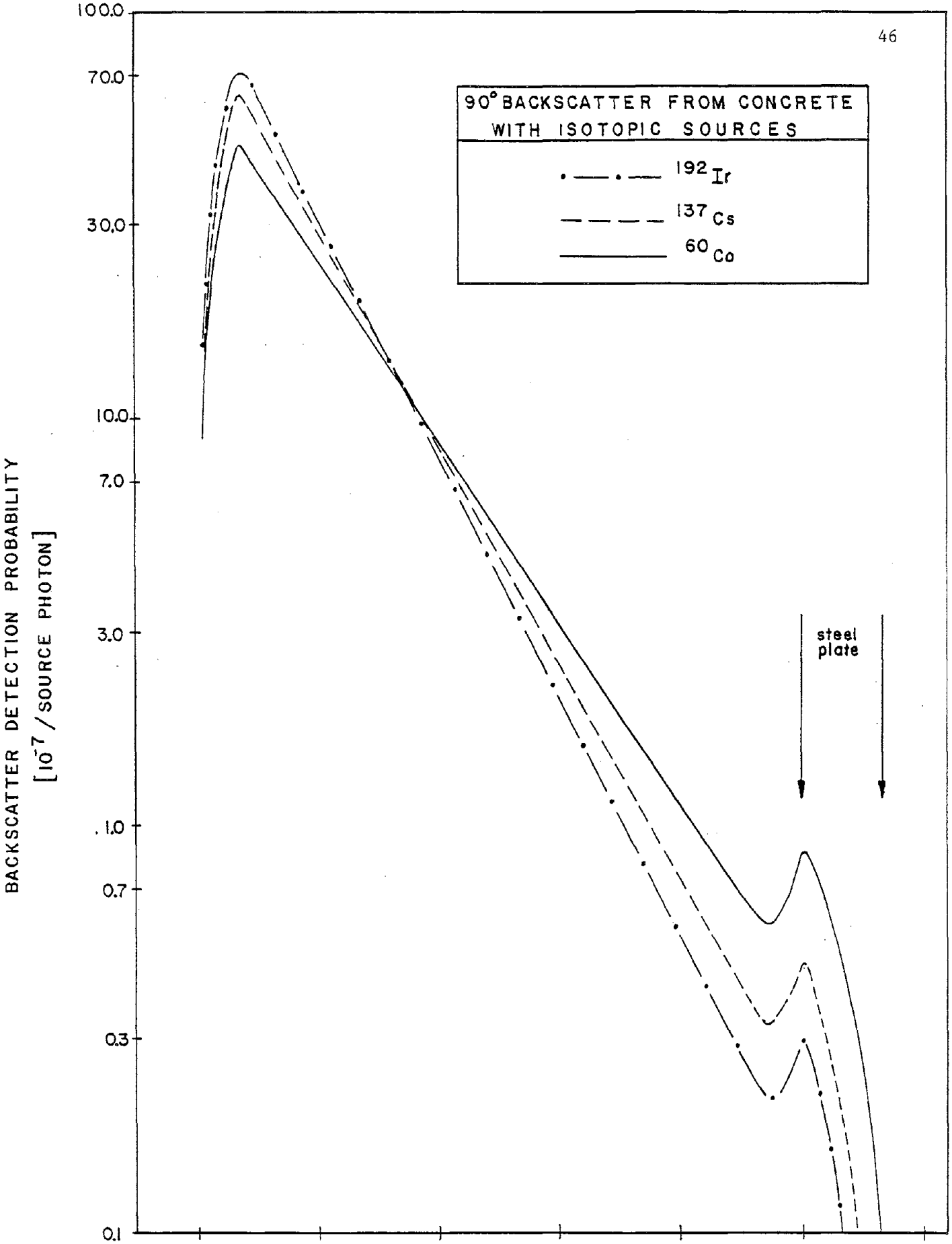

Fig. 27- POSITION OF CENTER OF SCATTER (CM)

gradually enters the front surface of the medium. The characteristic exponential drop in the signal as the depth increases is clearly displayed. The results of this experiment serve to provide a reference for comparing the results for situations where additional objects are embedded in the concrete medium.

(ii) A single 0.5" thickness steel plate was probed using the experimental setup described above. The purpose of this experiment was to obtain the trend of the backscatter signal as a function of the thickness probed and to exhibit the differential averaging effect. The results of this experiment provided an empirical determination of the focal volume extent. The results are shown in the Fig. 26, where the backscattered signal is plotted against the position.

(iii) A set of four experiments were performed to detect four rebars of diameters 0.95 cm, 1.3 cm, 1.9 cm, and 2.5 cm, respectively, embeddded in a concrete medium, 3.7 cm from the front surface. The signal strength as a function of the probe position in the medium was measured for each case and the results are shown in the Fig. 28. The initial shape in each case is identical and corresponds to the concrete medium alone. As the focal volume encounters the rebar region there is an increase in the signal due to the higher electron density corresponding to iron. As the focal volume moves past the rebar region a steeper drop in the signal, as compared to a uniform concrete medium, is due to the combined effect of the differential averaging as well as an increased attenuation arising from the passage of the beam through iron medium. Beyond the rebar region the signal resumes its characteristic exponentially decaying trend. It should be mentioned that as the focal volume moves deeper into the material, the signal tends to level off rather than reduce to zero. This is

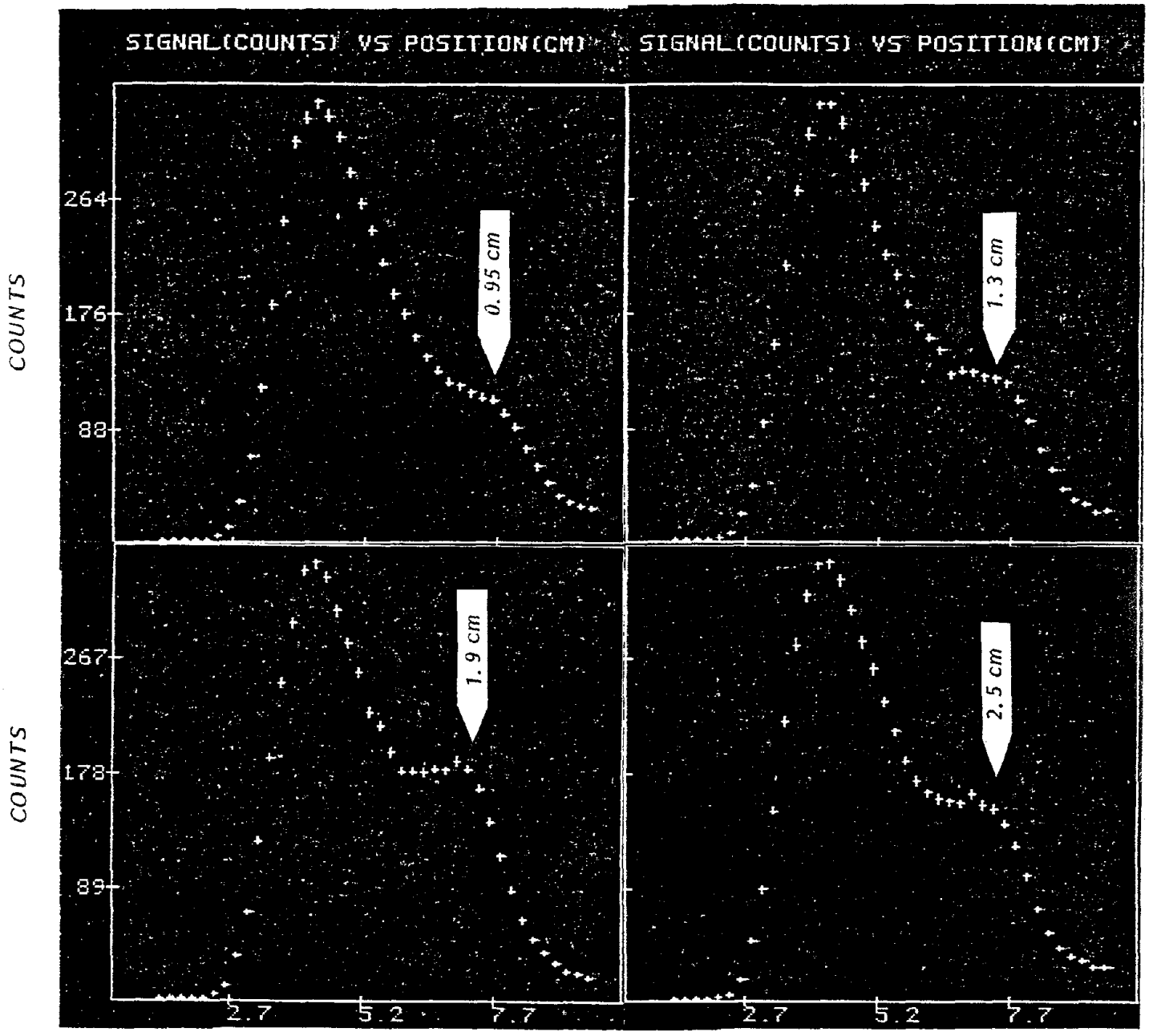

Fig. 28. Backscatter spectra from steel rebars of various diameters imbedded 3.7 cm inside a concrete block.

because the contributions from the background noise and the multiple scattering events dominate the primary signal at these depths.

(iv) An experiment was performed to detect the presence of a 1.5 cm diameter cylindrical air void located at 3.7 cm behind the front surface of a concrete medium. The results of this experiment are shown in the Fig. 29. In comparing with the signal trend for a unidrom concrete medium, a lowered value of the signal is obtained at the location of the air void. The signal is lower because the electron density of air is lesser than that for concrete. Similar deviation from the concrete medium signal were shown in (ii), where the presence of rebars increased the signal strength. The effect of differential averaging is also evident in the present case. The signal tends to level off around $\sim$ 18 count/sec at increased depths due to the reasons explained in (ii) and provide an empirical estimate of the background noise and the multiple scattering contributions.

(v) A set of experiments was performed to make a comparative study of the behaviour of the backscattered signal in a concrete background material containing a 0.5" steel plate and a 0.5" air gap, both located at the same distance behind the front surface of the concrete. First a uniform concrete medium was probed and then the experiment was repeated with the steel plate and an air gap embedded within the concrete. The backscattered signal for each of these three cases is shown in the Fig. 30(a). The dotted vertical lines show the position of the gap (i.e. the steel plate or the air gap). A rise in the signal relative to the concrete for the steel and a decrease for the air gap due to the relative electron density differences are clearly displayed. Beyond the gap, the signal is lower than the background for the case of steel because of the addition attenuation offered by steel, whereas due to the lesser

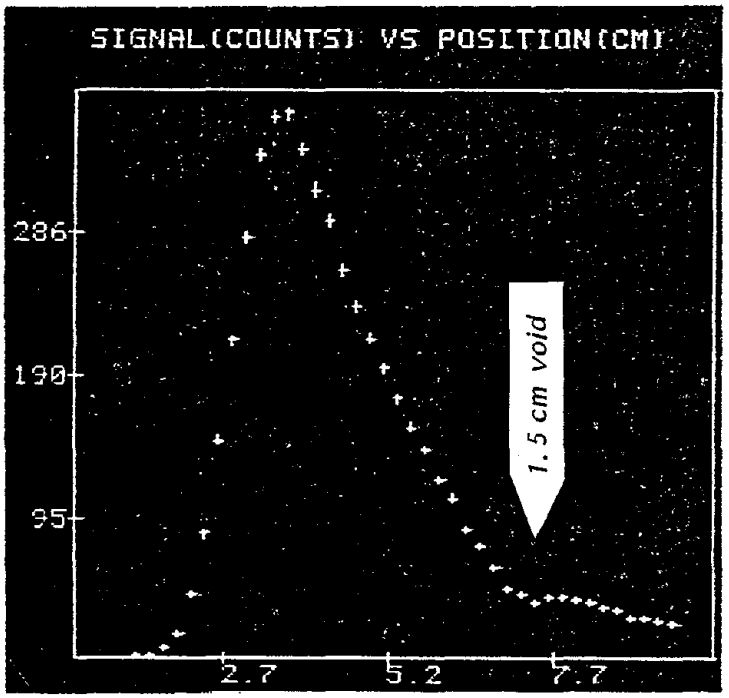

RELATIVE POSITION (cm)

Fig. 29. Backscatter scan for a concrete block with a 1.5 cm void located 3.7 cm from the front surface.

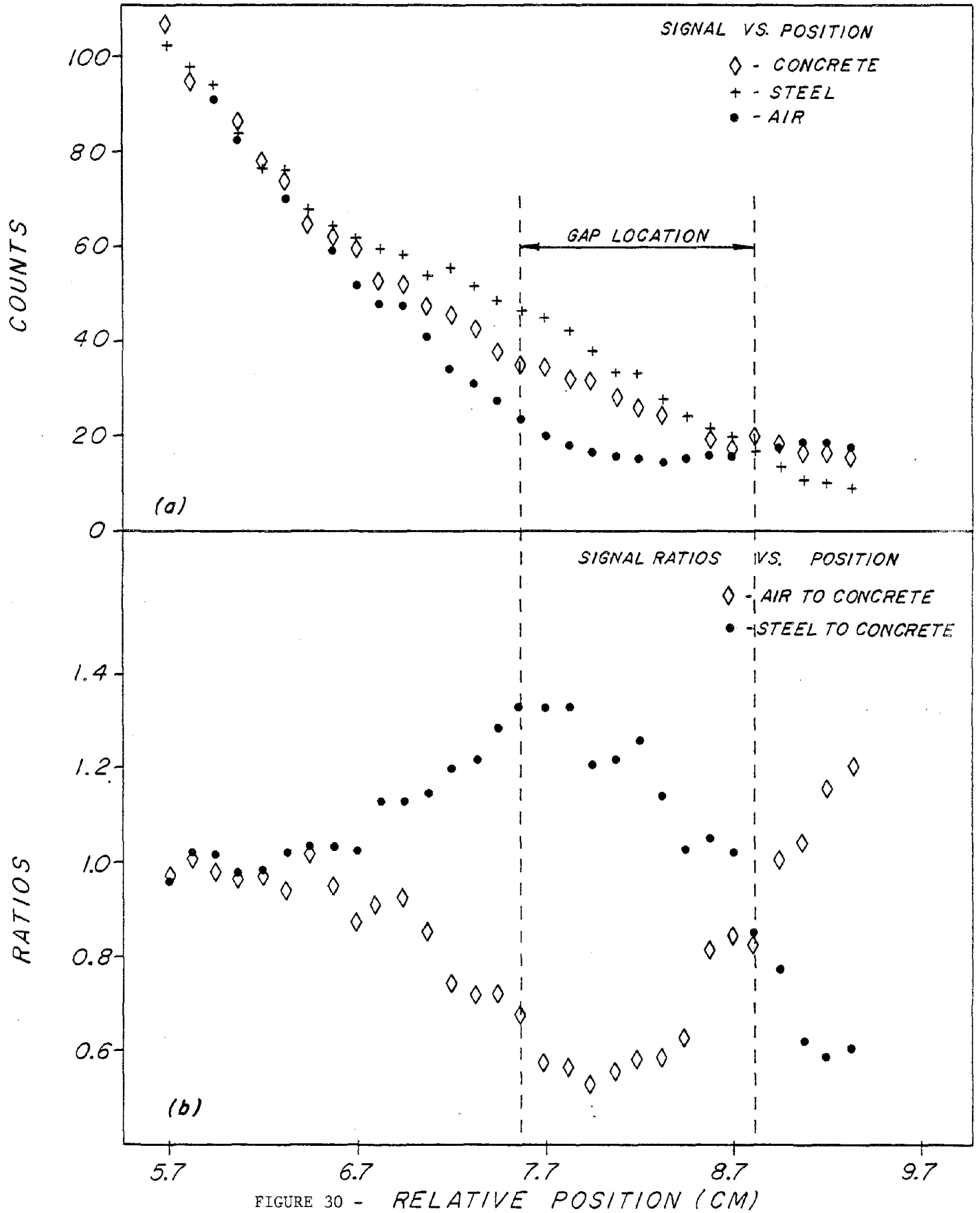
SIGNAL VS. POSITION
◇ - CONCRETE
+ - STEEL
● - AIR
GAP LOCATION
COUNTS
100
80
60
40
20
0
(a)
SIGNAL RATIOS VS. POSITION
◇ - AIR TO CONCRETE
● - STEEL TO CONCRETE
RATIOS
1.4
1.2
1.0
0.8
0.6
(b)
5.7
6.7
7.7
8.7
9.7
RELATIVE POSITION (CM)

FIGURE 30 -

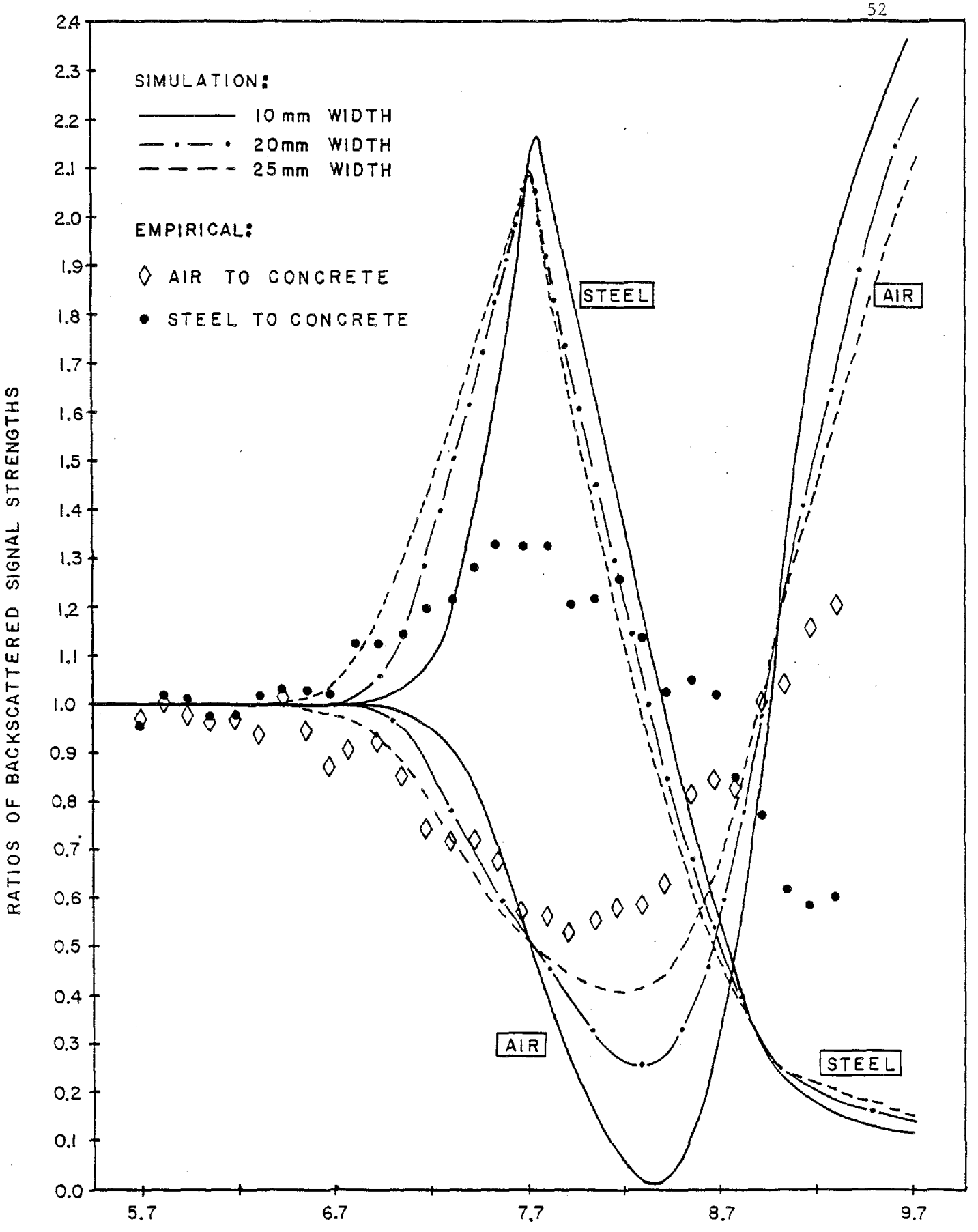

Fig. 31-RELATIVE POSITION (CM)

attenuation offered by air the corresponding signal is greater than the concrete case. In the Fig. 30(b) the ratios of the signal counts for the air gap and the steel plate cases, with respect to the concrete are plotted as a function of the relative position. The effects of the differential averaging as well as the attenuation characteristics of the "target" materials on the relative counts are clearly displayed. This experimental study was supplemented with a simulation study where only the focal volume extent was varied. The results of this simulation study are shown in the Fig. 31 with the experimental data superposed on it. The simulation study did not include any contributions of the noise or the contributions arising from multiple scatterings.

5. Conclusions

During this research a study was conducted to establish the feasibility of the computerized tomographic processes and the Compton interaction tomographic processes for their use as rapid, efficient and accurate nondestructive testing and evaluation techniques. The specific goal was to evaluate tomographic inspection of the condition and integrity of concrete structures, in general, to anticipate durability in event of earthquake and also after earthquake to determine damage.

The study of CT techniques was conducted on a specially fabricated phantom designed to include features commonly found in concrete structures such as walls and supports. These included steel rebars, air voids, air crack and background media composed of aggregate-sand mixture and concrete. The range of mass densities thus incorporated was from $\sim$ 0.0 gm/cc (air) up to 7.87 gm/cc (steel). The dimensions of the features varied from 1/16" to 18". The tomographic examinations of this object included scanning of the object subject to various selections of the tomographic parameters and reconstructions of the object cross-sectional mass distribution profiles known as Tomograms. The tomographic parameters varied were the number of angular views, the ray spacings in the photon fan beam and the degree of the detector collimation. For the entire tomographic study the isotopic photon source was selected to be a 50 Ci ^{60}Co source. A separate study was conducted to include the situations where a complete 360° tomographic access is not available. Tomographic scans were performed on the object with the viewing range limited to 135° and 90°, respectively. In each case two different degrees of collimation were employed.

The results of tomographic study are very encouraging, in that even for the worst parametric case composed of 80 angular views, 9.3 mm ray spacings

and 6.4 mm collimation, the phantom features such as the 1/4" rebar and the 1/4" air void are quite clearly distinguishable. The resolution of all of the features definitely improves as the number of angular views are increased and the ray spacings are made finer. Collimation influences the quality of the tomogram in that the finer the degree of collimation, the finer the sampling extent and hence the resolution of the finer features improves. It has an added advantage of reducing the noise arising from the scattered radiation. The study clearly establishes the criteria for the selection of the tomographic parameters as a function of the feature characteristic sought, and permits a rapid tomographic examination without an undue reduction in the resolution.

The study conducted for the limited view tomographic examination provided some useful results pertinent to earthquake engineering. Eventhough the amount of information obtained in a partial view scan is limited, it can suffice to indicate the presence of features depending on their extent and/or density. Thus we notice from both the 135° and the 90° partial scans that the rebars, the density of which is sufficiently higher than the background medium are detected in spite of the limited amount of information. This is indicative of the fact that in situations where the characteristics of the features sought after are known, a limited view tomographic scan can provide a rapid detection. It should be pointed out at this stage that no use of a priori information regarding the system was made in reconstructing the partial view tomograms. A priori information such as the geometry, the composition etc. of a feature can substantially aid in improving the quality of the tomogram. This effort, however, has been beyond the scope of the present research. In summary, the Computerized Tomographic techniques show a great promise for being nondestructive testing and evaluation methods. The flexibility of the tomographic parameter

in conjunction with the degree of resolution desired can, in many cases, yield an accurate assessment of the object system in relatively very short times. In particular, the initial results of the limited view studies indicate the feasibility of the applications of partial view tomography for the testing and evaluation of extended objects. With more research incorporated, such as inclusion of the a priori available information on the object system, this approach to investigating extended systems may well prove to be indispensable.

The feasibility of the Compton Interaction Tomography was investigated on a specially built apparatus. The possibility of the use of CIT processes for probing a medium to obtain information on its interior is known in principle. The experiments conducted here, of a limited nature due to source strength and intensity, exhibited qualitative agreement with appropriate simulation programs indicating the latter can be very valuable in obtaining estimates for other cases. They also indicated ^{192}Ir itself can be useful for limited depth backscattering measurements. The results indicate the potential feasibility of its application to massive systems such as concrete structural components.

The experiments were conducted using a 25 Ci - ^{192}Ir isotopic photon source and detection of features, such as rebars and air voids embedded in concrete background was assessed. Results of these initial laboratory studies indicate the possibility of the application of the CIT processes to massive extended structures. The features such as rebars and the air void were well discriminated from the concrete background, and even further improvement is envisioned if the use of higher energy and higher flux isotopic sources is made with high resolution detectors such as the Geli semiconductor detector. The higher energy sources will allow inspection at greater depths than possible with the ^{192}Ir. The preliminary study here serves to well establish the proof

of the principle. In addition, investigations of its applicability to massive systems are warranted.

In final conclusion, the Computerized tomographic processes appear well suited for the nondestructive testing and evaluation of massive objects such as reinforced concrete components integral to many massive structures. The results obtained support the viability of these techniques in providing accurate information. The tomographic processes permit a substantial degree of flexibility in selection of spatial resolution for rapid testing and evaluation. With the aid of pertinent a priori information on the system, these processes can be equally efficiently applied to extended objects prohibiting a complete 360^{o} access.

The preliminary results have also indicated that Compton interaction tomography (CIT), based on detection of backscattered photons, is a promising technique for detection of damage and defects such as delaminations, cracks, voids etc. in extended systems such as airport runways, highways, walls etc.